



Rheology of melts from the colli albani volcanic district (Italy): a case study

Christin Kleest¹ · Sharon L. Webb¹ · Sara Fanara¹

Received: 21 December 2019 / Accepted: 21 July 2020 / Published online: 14 August 2020
© The Author(s) 2020

Abstract

In this study the first viscosity measurements in the glass transition range of melts from highly explosive large-volume eruptions from the Colli Albani Volcanic District (CAVD) are presented. The magmas are ultrapotassic, rich in iron and CaO and characterised by a low silica content (<45 wt%). Melt compositions range from tephri-phonolitic to foiditic. The Colli Albani eruptions appear anomalous since they produced a large volume of erupted material in spite of their silica undersaturated compositions. The viscosity of the Colli Albani melt changes as the melt composition evolves from the original melt to a country-rock contaminated melt to a crystal-bearing melt with a permanent decrease in liquid viscosity. Conventional estimations of viscosities assume these magmas to have a low viscosity. The presented data show that the melt viscosities are higher than expected. Taking into account further chemical or rheological features of a melt, the investigated CAVD melts are not that striking as assumed in comparison with other large-volume eruptions. Consequently, considering the alkaline-earth to alkaline ratio together with the SiO₂ content could provide an alternative when comparing large volume eruptions.

Keywords Viscosity · Anhydrous melts · Colli Albani · Foidite · Glass transition · Low temperature

Introduction

Rheology of magma has an enormous influence on the eruptive style of volcanoes as well as mass transfer in magmas or crystallisation and degassing processes in cooling melts. The rheology of a magma depends on composition X, temperature T, pressure P, the content of crystals, bubbles and vesicles, oxygen fugacity, strain-rate and strain-rate induced crystallisation (i.e. Caricchi et al. 2007; Vona et al. 2011; Campagnola et al. 2016). Understanding eruption processes requires data at the appropriate P–T- and X conditions or modelling of the rheological and thermodynamic behaviour of melts using experimentally determined viscosity, heat capacity and configurational entropy data (e.g. Webb 2008; Russell and Giordano 2017).

In general, there is a positive correlation between the SiO₂ content and the viscosity of a melt, and highly viscous melts with a high silica content show typically an explosive eruptive style (Freda et al. 2011 and references therein). As shown by Freda et al. (2011), a way to illustrate the relationship between the erupted magma volume (a proxy for Volcanic Explosivity Index) and composition is to plot dense-rock equivalent (DRE) vs SiO₂ wt% (Fig. 1). On this plot, the magmas of Pozzolane Rosse and Pozzolane Nere, characterised by a low silica content, constitute two striking exceptions. These events belong to the Colli Albani Volcanic District (CAVD) located about 20 km south of Rome. The CAVD is part of the ultrapotassic Roman Volcanic Province, a volcanic belt parallel to the coast of the Tyrrhenian Sea and extending from southern Tuscany to central Latium (Peccerillo 2005). In its eruptive history, the CAVD had shown mainly explosive activity resulting in pyroclastic flow deposits accompanied by minor effusive activity that produced lava flows. In general, the products of the CAVD are characterised by a strong silica undersaturation and a high K content, shown in the TAS diagram in Fig. 2. The history of the CAVD is subdivided in three main periods characterised by dynamically different eruptive events (i.e. Karner et al. 2001; Giordano et al. 2006). The eruptions

Communicated by Mark S. Ghiorso.

✉ Christin Kleest
christin.kleest@uni-goettingen.de

¹ Georg August Universität Göttingen, Abteilung Experimentelle Mineralogie, Goldschmidtstraße 1, 37077 Göttingen, Germany

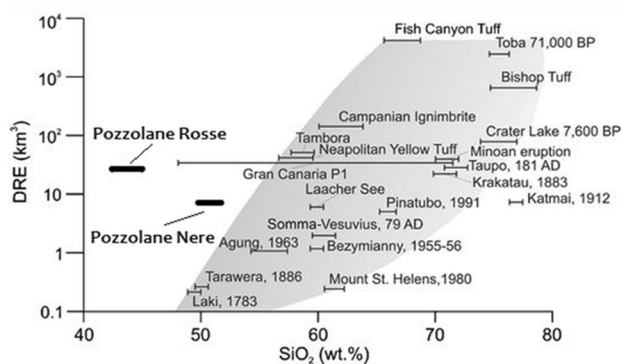


Fig. 1 Dense-rock equivalent (DRE) vs SiO₂ content showing the positive correlation between SiO₂ content and erupted volume with the exceptions of the Pozzolane Rosse and Pozzolane Nere events from the CAVD (after Freda et al. 2011 and references therein)

studied here belong to the earliest and most explosive phase: the Tuscolane-Artemisic phase (dated approx. 561–351 ka BP) (Karner et al. 2001), in which at least five of the largest pyroclastic flows were emplaced. The Pozzolane Rosse (PR) eruption with foiditic composition dated 456 ± 3 ka (Marra et al. 2009) and the tephri-phonolitic Pozzolane Nere (PN) eruption dated 407 ± 4 ka (Giordano et al. 2006) are the two largest eruptions of the CAVD. In spite of their low silica content, the PR and PN eruptions showed a highly explosive eruptive style. A low silica concentration and a high alkali

content, in general (Fig. 2), implies a low viscosity melt which should result in an effusive eruption (i.e. Freda et al. 2011; Campagnola et al. 2016).

The magma chamber of the CAVD is seated in a thick Mesozoic-Cenozoic carbonate wall rock with depths up to 7–8 km (Chiarabba et al. 1997; Giordano et al. 2006; Iacono-Marziano et al. 2007a). Previous studies (i.e. Iacono-Marziano et al. 2007a; Freda et al. 2008; Boari et al. 2009) suggested that significant assimilation of these carbonate rocks into the magma chamber resulted in a liberation of CO₂ which consequently led to the generation of a CO₂-rich melt with the rate of carbonate assimilation depending on melt viscosity (Bluythe et al. 2015). Moreover, an excess of CO₂ is thought to trigger an explosive eruption (Iacono-Marziano et al. 2007a; Boari et al. 2009; Freda et al. 2011; Di Rocco et al. 2012). Fragments of mainly leucite, but also amounts of clinopyroxene and biotite are found in the pyroclastic units of the PR and PN eruptions (Giordano et al. 2006; Freda et al. 2011). The presence of these crystals in the magma chamber would have increased the viscosity of the magma and thus increased the probability of an explosive eruptive event (Freda et al. 2011; Campagnola et al. 2016). Therefore, previous investigations on the Colli Albani volcano concentrated on the effects of carbonate assimilation and the crystal content. Campagnola et al. (2016) investigated the viscosities of pure liquid and crystal-bearing products from the PN event from the CAVD. The samples were

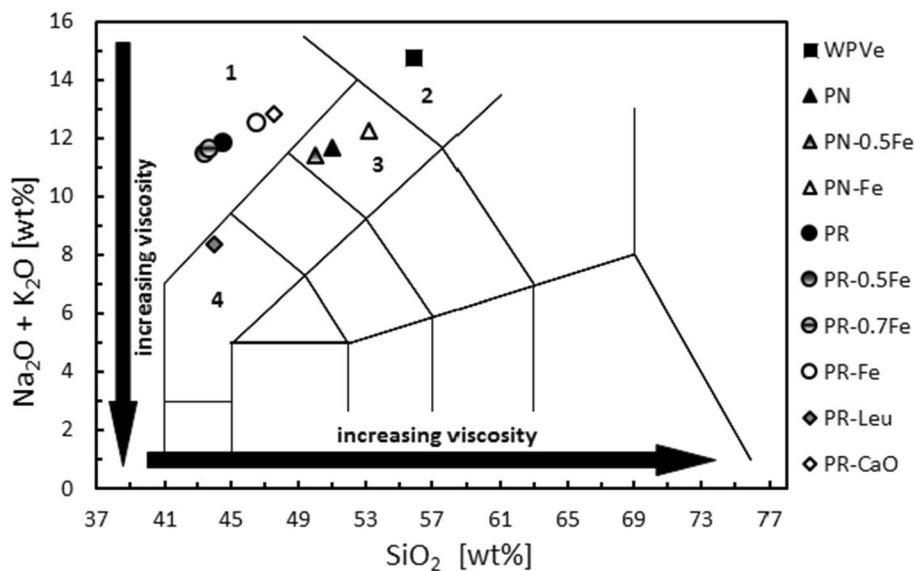


Fig. 2 TAS diagram with the compositions of the investigated melts with WPVe for White Pumice from the Vesuvius AD 79 eruption and composition after Iacono-Marziano et al. (2007b), PN for the Pozzolane Nere eruption from Colli Albani and composition after Campagnola et al. (2016), PN-0.5Fe for the modified PN composition with the half amount of iron, PN-Fe for the modified PN composition without iron, PR for the Pozzolane Rosse eruption from Colli Albani and composition after Freda et al. (2011), PR-0.5Fe for the

modified PR composition with the half amount of iron, PR-0.7Fe for the modified PR composition with 30% of iron, PR-Fe for the modified PR composition without iron, PR-Leu for the PR composition minus 4 mol % KAlSi₃O₆ and PR-CaO for the PR composition minus 7 wt% CaO and 1- foidite, 2- phonolite, 3- tephri-phonolite, 4- tephrite. Arrows indicate conventional estimations for the viscosity of a magma

remelted from natural material of a tephri-phonolitic composition at superliquidus conditions (for crystal-free melts) and subliquidus conditions (for crystal-bearing melts). The experimental measurements demonstrated that the viscosities at lower temperatures are higher than expected.

In this study, the first viscosity measurements of melt compositions from both the PR and PN event of the CAVD are presented to study their rheological features at sub-liquidus conditions in the glass transition range. Five different compositions are investigated: the K-foidite of the Pozzolane Rosse eruption (PR) with the composition taken from Freda et al. (2011), and another K-foidite that is calculated with the original PR composition minus 7 wt% CaO to represent the viscosity of the melt before its assimilation of the carbonate wall rocks (PR-CaO). To investigate the rheology of the melt after leucite crystallization, 4 mol % KAlSi_2O_6 were subtracted from the whole rock composition which results in a tephrite basanite (PR-Leu). The fourth composition is the tephri-phonolite from the Pozzolane Nere eruption (PN) with the whole rock composition of Campagnola et al. (2016). In addition, the more silicic “white pumice” phonolite from the Vesuvius AD 79 eruption (WPVe) (Iacono-Marziano et al. 2007b) is investigated to represent the acid end-member of the K-rich volcanism of central Italy.

Starting materials

Synthetic glasses with the composition of the PR and PN events from the CAVD as well as the modified compositions of PR-Leu and PR-CaO and the WPVe from the Vesuvius AD 79 eruption were prepared from powdered oxides and carbonates of SiO_2 , Al_2O_3 , Na_2CO_3 , TiO_2 , Fe_2O_3 , MnO , MgO , CaCO_3 and K_2CO_3 previously dried at 500 °C for 12 h with the exception of MgO that was dried at 1000 °C. The mixed powders were decarbonated at a slow heating rate to 1000 °C overnight. The mixture was melted in a $\text{Pt}_{90}\text{Rh}_{10}$ crucible for 1 h at 1600 °C and quenched by dipping the crucible in water. To improve the homogenisation, the melts were crushed and remelted twice for 1 h before the last melting at 1600 °C for 4 h. Both optical microscopy and microprobe analysis demonstrated the starting glasses were free of bubbles and crystals. Extra glasses of PN and PR were synthesized with lower amounts of iron to avoid effects of crystals growing during viscosity measurements. A second PN composition was synthesized with half the original iron content (PN-0.5Fe), and two extra PR melts were synthesized with half the amount of iron (PR-0.5Fe) and with 30% of its iron (PR-0.7Fe). Another set of PR and PN glasses were made iron-free (PR-Fe and PN-Fe, respectively). The composition of these melts were calculated based on the iron ratio ($\text{Fe}^{2+}/\text{Fe}_{\text{tot}}$) of the iron-bearing melts, and the ferric iron was replaced by Al^{3+} and the ferrous iron was replaced

by Mg^{2+} . The chemical compositions and iron ratios of all glasses investigated in this study are shown in Table 1.

Micropenetration technique

Viscosities η were determined in the range $10^{8.5}$ – $10^{13.5}$ Pa s using the micropenetration method. The measurements were carried out with a Netzsch TMA 402 Dilatometer. Glass discs, 3 mm thick, were polished to give 2 parallel faces before measurements. Depending on the viscosities, the duration of the measurements varied between 30 min and 3 h within a temperature range of 630–810 °C. The measurements were done in air in a sequence that alternates between lower and higher temperatures to ensure that the determined viscosity was not affected by crystallisation. The temperature in the dilatometer was calibrated to ± 0.5 °C with the melting points of Bi (268.02 °C), Zn (417.02 °C), Al (659.02 °C), NaCl (800.05 °C) and Ag (951.09 °C). The standard glass DGG1, a Na_2O – CaO – SiO_2 float glass from the Deutsche Glastechnische Gesellschaft was used to determine the precision of the dilatometer which is $\pm 0.06 \log_{10}$ Pa s. Hence, the total error of $\pm 0.06 \log_{10}$ Pa s (1σ) is assigned for each measured viscosity. A polished sphere of single crystal Al_2O_3 with 2 mm diameter was forced into the discs using 0.1–1.5 N. Viscosity is calculated from the rate of penetration of the sphere into the melt by:

$$\eta = \frac{0.1875Ft}{r^{0.5}l^{1.5}}, \quad (1)$$

with F —the applied force, t —time, r —radius of the indent sphere, l —distance of indent (Pocklington 1940; Tobolsky and Taylor 1963; Dingwell et al. 1992). Indent data obtained for timescales less than 100 τ (τ —relaxation time) after the application of the force were not included in the determination of viscosity.

Differential scanning calorimetry

The heat capacities were measured in a Netzsch DSC 404C differential scanning calorimeter in an argon atmosphere. Discs of the samples with polished parallel surfaces and weights between 5 and 82 mg were first heated to a temperature of about T_g^9 (the temperature at which the viscosity is 10^9 Pa s) with a rate of 20 °C min^{-1} and cooled with the same rate. The heat capacity of these glasses with a fictive temperature set by the 20 °C min^{-1} cooling rate were then measured at a 20 °C min^{-1} heating rate. The samples in a Pt crucible were measured against an empty Pt crucible. The calibration of the calorimeter was done with a single sapphire crystal ($m = 113.140 \pm 0.005$ mg) and the heat capacity data of Robie et al. (1978). The error of the measurements is $\leq 1\%$. The configurational heat capacity (C_p^{conf}) was calculated as the difference between the liquid heat capacity (C_{pl})

Table 1 Chemical compositions of the investigated melts determined by electron microprobe analysis (JEOL JXA 8900 RL) with 15 kV acceleration voltage, 15 nA current and 25 μm beam diameter. Listed data are the average of 20 single measurements (in wt%). Standard deviation is 1σ . The data in mol% are calculated using the atomic analysis combined with the Fe-ratio determined by colorimetric micro-determination, here the standard variation is 2σ

Electron microprobe analysis												
[wt%]	SiO ₂	Al ₂ O ₃	Na ₂ O	TiO ₂	FeO	MnO	MgO	CaO	K ₂ O	Total	Fe ²⁺ /Fe _{tot}	M [g mol ⁻¹] ^a
WPVe	55.91 ± 0.16	21.47 ± 0.10	5.29 ± 0.08	0.30 ± 0.02	2.72 ± 0.05	0.13 ± 0.03	0.41 ± 0.02	3.25 ± 0.05	9.48 ± 0.08	98.96	0.42 ± 0.02	69.44
PN	51.02 ± 0.16	19.47 ± 0.10	2.54 ± 0.06	0.64 ± 0.02	7.28 ± 0.09	0.19 ± 0.03	2.37 ± 0.04	5.56 ± 0.06	9.13 ± 0.08	98.20	0.44 ± 0.02	69.50
PN-0.5Fe	50.01 ± 0.16	22.41 ± 0.10	2.50 ± 0.06	0.63 ± 0.02	5.82 ± 0.08	0.19 ± 0.02	3.25 ± 0.03	5.47 ± 0.06	8.92 ± 0.08	99.20	0.44 ± 0.03	69.42
PN-Fe	53.24 ± 0.15	22.48 ± 0.10	2.62 ± 0.06	0.68 ± 0.02	–	–	4.61 ± 0.05	5.72 ± 0.06	9.62 ± 0.08	98.97	–	67.06
PR	44.42 ± 0.15	16.46 ± 0.09	3.17 ± 0.06	0.93 ± 0.02	9.46 ± 0.10	0.20 ± 0.03	3.94 ± 0.05	10.82 ± 0.09	8.73 ± 0.08	98.13	0.39 ± 0.01	68.08
PR-0.5Fe	43.30 ± 0.15	19.84 ± 0.10	3.04 ± 0.06	0.92 ± 0.04	7.46 ± 0.09	0.20 ± 0.02	5.44 ± 0.04	10.55 ± 0.09	8.47 ± 0.08	99.22	0.36 ± 0.03	68.22
PR-0.7Fe	43.62 ± 0.15	21.46 ± 0.10	3.10 ± 0.06	0.92 ± 0.04	5.10 ± 0.07	0.21 ± 0.02	5.45 ± 0.04	10.71 ± 0.09	8.58 ± 0.08	99.15	0.37 ± 0.02	67.83
PR-Fe	46.47 ± 0.15	20.41 ± 0.10	3.22 ± 0.06	1.02 ± 0.03	–	–	6.87 ± 0.07	11.25 ± 0.09	9.37 ± 0.08	98.61	–	65.35
PR-Leu	43.95 ± 0.15	15.80 ± 0.09	3.71 ± 0.07	1.11 ± 0.03	11.13 ± 0.10	0.25 ± 0.03	4.63 ± 0.05	12.82 ± 0.09	4.66 ± 0.06	98.06	0.42 ± 0.02	67.34
PR-CaO	47.57 ± 0.15	17.68 ± 0.09	3.42 ± 0.07	1.04 ± 0.03	10.25 ± 0.10	0.23 ± 0.03	4.23 ± 0.05	4.26 ± 0.05	9.44 ± 0.08	98.12	0.42 ± 0.01	69.62
Calculated compositions												
[mol%]	SiO ₂	Al ₂ O ₃	Na ₂ O	TiO ₂	FeO	Fe ₂ O ₃	MnO	MgO	CaO	K ₂ O	γ^b	
WPVe	65.18 ± 0.32	14.75 ± 0.12	5.98 ± 0.15	0.26 ± 0.03	1.11 ± 0.03	0.77 ± 0.03	0.13 ± 0.05	0.71 ± 0.06	4.06 ± 0.11	7.05 ± 0.10	0.55	
PN	59.81 ± 0.29	13.46 ± 0.11	2.88 ± 0.11	0.57 ± 0.03	3.14 ± 0.06	2.00 ± 0.03	0.19 ± 0.05	4.14 ± 0.11	6.99 ± 0.12	6.83 ± 0.09	0.61	
PN-0.5Fe	58.03 ± 0.31	15.33 ± 0.12	2.81 ± 0.09	0.55 ± 0.04	2.49 ± 0.05	1.58 ± 0.04	0.18 ± 0.03	5.62 ± 0.09	6.80 ± 0.13	6.61 ± 0.10	0.59	
PN-Fe	60.04 ± 0.32	14.94 ± 0.12	2.86 ± 0.12	0.58 ± 0.03	–	–	–	7.75 ± 0.16	6.91 ± 0.14	6.92 ± 0.11	0.62	
PR	51.29 ± 0.25	11.20 ± 0.09	3.55 ± 0.11	0.81 ± 0.03	3.57 ± 0.06	2.79 ± 0.04	0.19 ± 0.04	6.77 ± 0.13	13.39 ± 0.16	6.43 ± 0.09	0.71	
PR-0.5Fe	49.29 ± 0.26	13.31 ± 0.10	3.35 ± 0.10	0.79 ± 0.05	2.56 ± 0.04	2.27 ± 0.04	0.19 ± 0.03	9.23 ± 0.10	12.86 ± 0.17	6.15 ± 0.09	0.69	
PR-0.7Fe	49.49 ± 0.27	14.35 ± 0.10	3.41 ± 0.10	0.78 ± 0.05	1.79 ± 0.04	1.52 ± 0.03	0.20 ± 0.03	9.22 ± 0.11	13.02 ± 0.17	6.21 ± 0.09	0.68	
PR-Fe	51.26 ± 0.28	13.27 ± 0.11	3.44 ± 0.11	0.85 ± 0.04	–	–	–	11.30 ± 0.19	13.30 ± 0.18	6.59 ± 0.09	0.72	
PR-Leu	49.86 ± 0.25	10.56 ± 0.09	4.09 ± 0.11	0.95 ± 0.04	4.43 ± 0.06	3.06 ± 0.04	0.25 ± 0.04	7.84 ± 0.12	15.59 ± 0.16	3.37 ± 0.08	0.72	
PR-CaO	55.80 ± 0.26	12.22 ± 0.10	3.89 ± 0.12	0.92 ± 0.04	4.22 ± 0.06	2.92 ± 0.05	0.23 ± 0.04	7.39 ± 0.13	5.35 ± 0.11	7.07 ± 0.09	0.65	

^aM is calculated by normalising the total weight of each oxide to one mole of the sample

$$\gamma = \frac{\text{Ni}_2\text{O} + \text{K}_2\text{O} + \text{CaO} + \text{MgO} + \text{FeO}}{\text{Ni}_2\text{O} + \text{K}_2\text{O} + \text{CaO} + \text{MgO} + \text{FeO} + \text{Al}_2\text{O}_3 + \text{Fe}_2\text{O}_3}$$

and the glass heat capacity (C_{pg}) extrapolated to the same temperature as the liquid heat capacity. The heat capacity of the glass (c_{pg}) is determined by the extrapolation of the Maier-Kelley-Fit to the unrelaxed glass heat capacity:

$$c_{pg} = a + bT + cT^{-2}, \quad (2)$$

with a , b and c as parameters and T —temperature in Kelvin (Maier and Kelley 1932).

Determining the heat capacities of all of the melts (c_{pl}) is not possible due to crystallisation during the measurements. Therefore, c_{pl} and C_p^{conf} are modelled after Giordano and Russell (2017) and Russel and Giordano (2017) as discussed below.

Colorimetric micro-determination of the iron species

The colorimetric micro-determination of the ferrous and ferric iron ratio in silicic glasses was first developed by Wilson (1960) and modified by Schuessler et al. (2008). This method involves measurement of the ferrous iron species by UV/VIS spectroscopy. Each sample is crushed and 4–10 mg of the powdered glass is dissolved in hydrofluoric acid (HF). The bivalent iron builds a reddish Fe(II)-bipyridyl-complex with 2:2'bipyridyl added to the solution that shows an intensive absorption band at approx. 523 nm. Measurements of the total iron content are obtained by reducing the ferric iron into the ferrous species with hydroxylamine hydrochloride (H_4NOCl). The total iron content of the sample is determined by comparing the absorption of the sample with a series of standards with known ferrous iron concentrations. UV/VIS measurements were done with an AvaSpec-UV/VIS/NIR spectrometer from Avantes and the software AvaSoft Version 8.3. The ratio of the ferrous to total iron in the sample is directly acquired from the ratio of the absorbances at 523 nm. The iron ratios Fe^{2+}/Fe_{tot} are given in Table 1.

Results and discussion

All the investigated melts are metaluminous defined by $Na_2O + K_2O < Al_2O_3 < CaO + MgO + Na_2O + K_2O$ in mole fraction (Shand 1927). An estimation of the degree of depolymerisation and hence of the melt structure is $\gamma = (Na_2O + K_2O + CaO + MgO + FeO) / (Na_2O + K_2O + CaO + MgO + FeO + Al_2O_3 + Fe_2O_3)$ in mole fraction (Toplis et al. 1997; Webb et al. 2007) which ranges from 0.55 for WPVe to 0.72 for PR-Fe and PR-Leu. The γ values are given in Table 1.

The iron ratio (Fe^{2+}/Fe_{tot}) was found to be in the range from 0.36–0.44 (see Table 1). All samples were synthesised at the same temperature (1600 °C) and oxygen fugacity (in

air) and were quenched at the same rate at 0.1 MPa. Kress and Carmichael (1991) developed a model for the calculation of the iron ratio of silicate melts in dependence of composition, temperature, oxygen fugacity and pressure. A comparison with the Fe^{2+}/Fe_{tot} calculated by this model and the measured Fe^{2+}/Fe_{tot} shown in Fig. 3 illustrates that the modelled iron ratios are within the error of the measured values, showing this model works well for the studied melt compositions.

Viscosity

The samples investigated in this study were found to be free of bubbles and crystals by optical microscopy and scanning electron microscopy (SEM) with magnifications up to 10^6 times. However, Raman spectroscopy indicated the presence of nanolites. Figure 4 shows the Raman spectra for sample PR-CaO exhibiting the highest nanolite content represented by the peak at approx. 680 cm^{-1} belonging to magnetite with the clear glass “hump” in the area of approx. 950 cm^{-1} . This is in agreement with the observations from Di Genova et al. (2017) who recognised the effect of nanolites in Fe-bearing glasses on the Raman spectra. The ratio of the peaks is reduced after the viscosity measurements with respect to the spectra obtained before the viscosity measurements. This indicates an increase in the nanolite content. As due to the fact that the nanolites in the post-viscosity glasses are not visible in the SEM, they are assumed to be so small and unconnected that their presence would have an insignificant effect on the viscosity. Stevenson et al. (1996) showed that a crystal fraction of 1 vol% or less in homogenous distribution in the melt and without any connectivity has negligible influence on the viscosity. However, accounting the effect of crystallisation of magnetite depleting the residual melt in Fe_3O_4 , the viscosity of the chemically changed residual

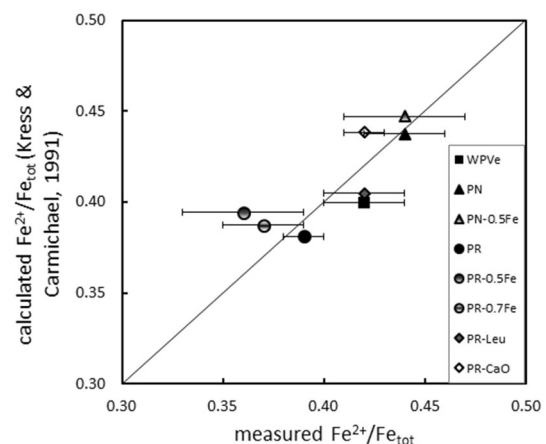


Fig. 3 Comparison of measured iron ratios with calculated iron ratios after Kress & Carmichael (1991) and the 1:1 line

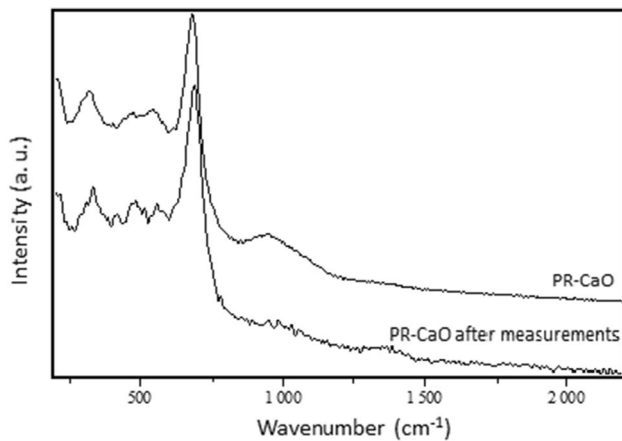


Fig. 4 Raman spectra of the sample PR-CaO. The upper spectrum is from the glass before viscosity measurements and the lower one is that from the glass after viscosity measurements

liquid is modelled with a crystal content of 2 vol% and discussed below.

Measured viscosities are listed in Table 2. The best fit for viscosity measurements over the present temperature range is the Arrhenius Equation

$$\log_{10}\eta = A + \frac{B \cdot 10^4}{T}, \quad (3)$$

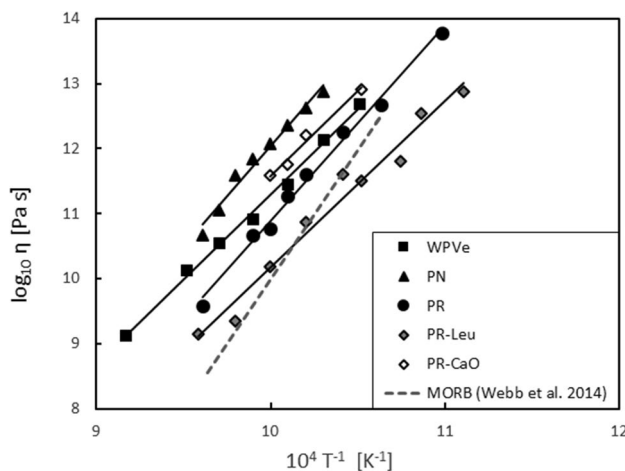
with A and B as fit parameters and T —temperature in Kelvin. An equation more complex than a straight line fit to $\log_{10} \eta$ as a function of inverse temperature is not statistically possible due to the small range in both viscosity and temperature over which the data are obtained. The fitted parameters of the Arrhenius Equation are given in Table 3. The measured viscosities for the melts with the original iron content of the whole rock composition are plotted in Fig. 5 as a function of inverse temperature. The viscosity data of a MORB melt (Webb et al. 2014) are plotted for comparison, showing that the MORB viscosity is lower than that of the foiditic PR and the tephri-phonolitic PN. At the fixed temperature of 700 °C, the most viscous melt from this study is the PN composition (12.89 \log_{10} Pa s) being nearly 1.2 orders of magnitude higher than that of PR (11.72 \log_{10} Pa s). PR-Leu is 0.85 \log_{10} Pa s lower than PR as expected since network formers are removed to form this melt composition. As a result of subtracting the network modifying CaO from PR (PR-CaO) the viscosity increases by 0.58 \log_{10} Pa s. At temperatures above 730 °C, the crystallisation, detected by optical microscopy and X-ray diffraction, affects the viscosity

Table 2 Measured viscosities at given temperatures. The error in viscosity is $\pm 0.06 \log_{10}$ Pa s, the error in temperature is ± 0.5 °C

WPVe		PN		PN-0.5Fe		PN-Fe		PR	
T [°C]	$\log_{10} \eta$ [Pa s]	T [°C]	$\log_{10} \eta$ [Pa s]	T [°C]	$\log_{10} \eta$ [Pa s]	T [°C]	$\log_{10} \eta$ [Pa s]	T [°C]	$\log_{10} \eta$ [Pa s]
678.3	12.68	697.2	12.87	702.6	13.1	682.5	13.34	637.2	13.78
697.3	12.13	707.3	12.62	717.7	12.72	702.6	12.44	667.2	12.68
717.3	11.45	717.3	12.36	732.8	12.02	722.7	12.09	687.2	12.26
737.3	10.91	727.3	12.07	742.8	11.89	732.8	11.72	707.3	11.60
757.3	10.54	737.3	11.84	752.9	11.39	743.0	11.38	717.3	11.27
777.3	10.12	747.3	11.59	763.0	11.14	783.3	10.12	727.3	10.77
817.3	9.13	757.3	11.05	773.1	10.89	803.3	9.59	737.3	10.66
		767.3	10.66	783.2	10.41	823.9	9.01	767.3	9.58
				803.3	10.09	843.5	8.58		
				813.4	9.89				
PR-0.5Fe		PR-0.7Fe		PR-Fe		PR-Leu		PR-CaO	
T [°C]	$\log_{10} \eta$ [Pa s]	T [°C]	$\log_{10} \eta$ [Pa s]	T [°C]	$\log_{10} \eta$ [Pa s]	T [°C]	$\log_{10} \eta$ [Pa s]	T [°C]	$\log_{10} \eta$ [Pa s]
652.2	13.61	642.2	13.40	642.2	13.61	627.2	12.88	677.3	12.91
672.4	12.87	662.3	12.80	702.6	11.82	647.2	12.54	707.3	12.21
697.5	12.00	682.4	11.97	722.7	10.85	657.2	11.81	717.3	11.75
712.6	11.25	702.6	11.19	742.9	10.29	677.2	11.51	727.3	11.58
722.7	10.97	712.6	10.86	763.0	9.59	687.2	11.61		
741.8	10.31	722.7	10.33	783.1	9.25	707.3	10.87		
752.9	9.81	742.9	9.59	803.3	8.28	727.3	10.19		
768.1	9.48	763.3	8.95			747.3	9.35		
783.2	9.13	783.4	8.41			767.4	9.14		
803.6	8.73								

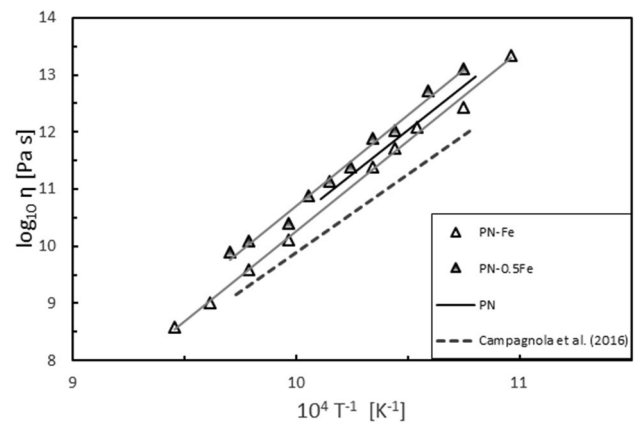
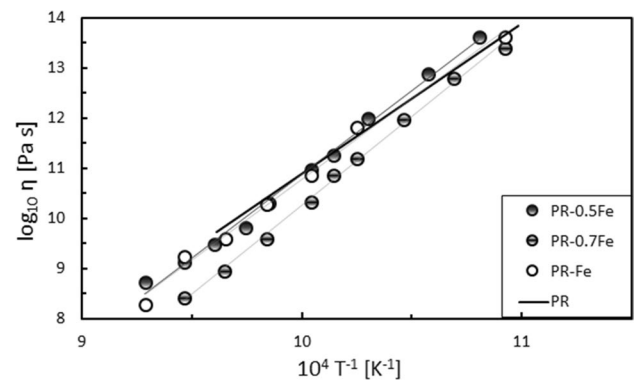
Table 3 Fit parameters from the Arrhenius Equation (Eq. 3) using the viscosity data and T_g^{12} and fragility m (Eq. 4)

	A [\log_{10} Pa s]	B [K]	T_g^{12} [K]	m
WPVe	-14.80 ± 0.06	2.61 ± 0.01	973.6	26.8
P.N.	-18.96 ± 0.45	3.10 ± 0.07	1001.1	31.0
PN-0.5Fe	-19.58 ± 0.19	3.19 ± 0.03	1009.4	31.6
PN-Fe	-19.69 ± 0.05	3.15 ± 0.01	995.0	31.7
PR	-19.13 ± 0.15	3.00 ± 0.02	964.2	31.1
PR-0.5Fe	-22.71 ± 0.10	3.36 ± 0.02	967.7	34.7
PR-0.7Fe	-25.24 ± 0.07	3.55 ± 0.01	953.1	37.2
PR-Fe	-21.43 ± 0.19	3.22 ± 0.03	963.2	33.4
PR-Leu	-15.24 ± 0.52	2.54 ± 0.09	932.9	27.2
PR-CaO	-14.26 ± 0.26	2.58 ± 0.05	984.2	26.3

**Fig. 5** Viscosities as a function of inverse temperature of the investigated melts with the original iron content in comparison with a MORB (dotted line) (Webb et al. 2014)

of PR-CaO, resulting in an increase in viscosity by nearly two orders of magnitude. Therefore, the data of obviously crystal bearing melts are not presented here. The melt with the highest SiO_2 content, WPVe, shows viscosities lying in the middle of the viscosity range of the investigated melt compositions. Thus, the viscosities of the investigated melts are not as low as assumed although they have a silica-poor and K-rich composition.

The viscosities of the PN series are presented in Fig. 6 and Table 2. The viscosity of PN-Fe is $\sim 0.5 \log_{10}$ Pa s lower than that of PN-0.5Fe and around $0.2 \log_{10}$ Pa s lower than the viscosity of PN with the original iron content. The viscosity data of the anhydrous remelted natural PN melt from Campagnola et al. (2016) are also shown in Fig. 6. The measured viscosities in this study are ~ 1 order higher than those from Campagnola et al. (2016). The Einstein-Roscoe viscosity model (Einstein 1906; Roscoe 1952) as well as that of Caricchi et al. (2007) require 35 vol% crystal content to

**Fig. 6** Viscosity data of the PN series ($0.59 < \gamma < 0.62$) as a function of inverse temperature. Dotted line are the viscosity data of PN measured by Campagnola et al. (2016)**Fig. 7** Viscosity data of the PR series ($0.68 < \gamma < 0.72$) as a function of inverse temperature

increase viscosity by one order of magnitude. Due to this discrepancy, the standard glass DGG1 was remeasured to confirm the accuracy of both the dilatometer measurements and the data evaluation.

The Arrhenius plots of the original and modified PR melts are shown in Fig. 7 and data are listed in Table 2. The PR-0.7Fe composition shows slightly lower viscosities over the whole viscosity range compared to the other PR melts with a deviation of $\sim 0.7 \log_{10}$ Pa s.

As illustrated in Fig. 8, which shows the glass transition temperature T_g^{12} (the temperature at which the viscosity is 10^{12} Pa s) as a function of γ , there is a decreasing trend of viscosity with increasing γ , with the exception of the WPVe melt which will follow a different compositional trend as it is poor in alkali-earth compared to the other melts. This T_g^{12} trend has been extensively discussed in the literature (i.e. Richet 1984; Toplis 1998; Webb et al. 2004, 2005, 2007) and is due to the increase in the amount of non-bridging oxygens as the bridging oxygens of the Si-O and tetrahedral Al-O

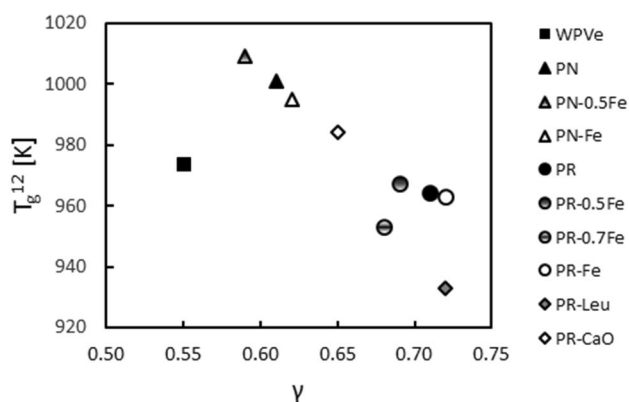


Fig. 8 T_g^{12} as a function of γ

bonds are broken by the network modifiers. This trend is generally observed within the investigated melt series of the CAVD in spite of relatively small variation in the viscosity within the PR composition series.

Fragility

Using the viscosity data the fragility m is calculated from the equation

$$m = \frac{B \times 10^4}{T_g^{12}}, \tag{4}$$

with B —parameter of the Arrhenius fit (Eq. 3) in Kelvin and T_g^{12} —temperature at which the viscosity is 10^{12} Pa s in Kelvin (Toplis et al. 1997; Webb 2011). The values of m and

T_g^{12} are reported in Table 3. Fragility is a value indicating the deviation from an Arrhenian behaviour. The series of PR compositions exhibit the highest fragilities (31.1 to 37.2), followed by the series of PN compositions (31.0 to 31.7), PR-Leu (27.2), WPVe (26.8) and PR-CaO (26.3).

Calorimetry

The fit parameters a , b and c of the Maier-Kelley Equation (Eq. 2) are shown in Table 4. For WPVe, PN-Fe, PR-0.7Fe and PR-Fe, a determination of c_{pl} is possible. It was not possible to obtain a c_{pl} value for the other melts due to crystallisation at the given temperature. As the value of C_p^{conf} is required in the Adam-Gibbs description of viscosity as a function of temperature (Adam and Gibbs 1965; Richet 1984, 1987; Toplis et al. 1997; Webb 2008), the relationship of Giordano and Russell (2017) is used to estimate C_p^{conf} .

Table 4 shows the calculated data. To treat all calorimetry data and resultant values equally, C_{pl} and C_p^{conf} are calculated for all investigated melts after Giordano and Russell (2017). However, these values have to be regarded as a first approximation of the heat capacities since the correlation from Giordano and Russell (2017) does not include foiditic, tephri-phonolitic or phonolitic compositions and it assumes the same iron speciation for all melts.

The calculated C_p^{conf} is plotted vs γ in Fig. 9. It shows a general positive correlation between γ and C_p^{conf} . WPVe with the lowest value of γ (0.55) has the lowest C_p^{conf} ($16.28 \text{ J mol}^{-1} \text{ K}^{-1}$). The highest values of C_p^{conf} are calculated for PR-0.5Fe and for PR-Leu ($25.78 \text{ J mol}^{-1} \text{ K}^{-1}$) with values of γ of 0.69 and 0.72, respectively. As pointed out by Giordano and Russell (2017) an increase in the SiO_2 content

Table 4 Heat capacity, configurational heat capacity, configurational entropy and the parameters for the Maier–Kelley Equation (Eq. 2)

	Maier–Kelley parameters							
	$a [\text{J g}^{-1} \text{ K}^{-1}]$	$b [\text{J g}^{-1} \text{ K}^{-2}]$	$c^* 10^3 [\text{J g}^{-1} \text{ K}]$	$c_{pg} [\text{J g}^{-1} \text{ K}^{-1}]$	$C_{pl} [\text{J mol}^{-1} \text{ K}^{-1}]^{(a)}$	$C_p^{conf} [\text{J mol}^{-1} \text{ K}^{-1}]^{(b)}$	$S_{conf} [\text{J mol}^{-1} \text{ K}^{-1}]^{(c)}$	$B_e [\text{kJ mol}^{-1}]^{(c)}$
WPVe	1.151 ± 0.001	35.47 ± 1.29	-48.72 ± 0.19	1.15	94.95	16.28	21.74 ± 1.34	779.50 ± 46.81
PN	1.229 ± 0.003	-75.05 ± 2.91	-57.99 ± 0.44	1.10	95.73	19.63	20.90 ± 3.03	774.16 ± 111.40
PN-0.5Fe	1.222 ± 0.002	-63.62 ± 1.75	-53.15 ± 0.27	1.11	97.46	20.75	19.99 ± 1.27	742.61 ± 46.37
PN-Fe	1.139 ± 0.002	79.61 ± 1.44	-47.50 ± 0.21	1.18	97.53	19.07	17.46 ± 0.90	638.70 ± 31.96
PR	1.158 ± 0.003	-15.76 ± 2.93	-49.16 ± 0.42	1.10	98.66	24.66	25.77 ± 2.39	918.35 ± 83.90
PR-0.5Fe	0.993 ± 0.010	134.48 ± 8.65	-63.02 ± 2.12	1.08	97.41	25.78	20.10 ± 0.82	714.09 ± 28.01
PR-0.7Fe	1.324 ± 0.002	-65.95 ± 2.11	-70.87 ± 0.29	1.19	105.46	25.22	17.26 ± 0.98	603.99 ± 33.14
PR-Fe	1.158 ± 0.003	39.51 ± 2.81	-54.16 ± 0.45	1.15	98.60	24.10	20.70 ± 2.20	730.95 ± 74.68
PR-Leu	1.021 ± 0.001	161.08 ± 1.62	-35.25 ± 0.22	1.15	102.14	25.78	33.06 ± 6.07	1141.00 ± 204.03
PR-CaO	1.257 ± 0.002	-92.47 ± 2.27	-57.62 ± 0.35	1.11	103.95	22.42	35.98 ± 9.17	1304.51 ± 331.79

^a C_{pl} calculated using C_p^{conf} after Giordano and Russell (2017)

^b C_p^{conf} calculated via $C_p^{conf} = 52.6 - 55.88X_{\text{SiO}_2}$ with X_{SiO_2} – mole fraction of the SiO_2 content of the melt (Giordano and Russell 2017)

^c S_{conf} and B_e fitted via Eq. 5

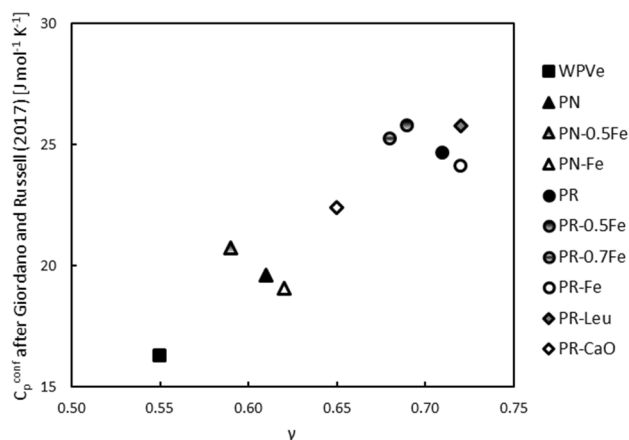


Fig. 9 C_p^{conf} as a function of γ . C_p^{conf} is estimated after $C_p^{\text{conf}} = 52.6 - 55.88X_{\text{SiO}_2}$ (with X_{SiO_2} – mole fraction of the SiO_2 content) showing an increase with increasing γ

of a melt leads to a decreasing C_p^{conf} . The same conclusion is reached by Russell and Giordano (2017) who concluded that an increasing SiO_2 accompanied with a rising degree of polymerisation would result in a less re-ordering of the melt structure at the glass transition and therefore a lower C_p^{conf} .

Combining the viscosity data and the calculated C_p^{conf} enables the evaluation of the configurational entropy (S_{conf}) using the Equation

$$\log_{10}\eta = A_e + \frac{B_e}{\ln 10 \left[S_{\text{conf}} \left(T_g^{12} \right) + \int_{T_g}^T \frac{C_p^{\text{conf}}}{T} dT \right]} T \quad (5)$$

(Richet 1984; Webb 2008; Falenty and Webb 2010) with A_e and B_e as constants, T —temperature in Kelvin and T_g^{12} —glass transition temperature in Kelvin, conventionally assumed as the temperature at which the viscosity is 10^{12} Pa s. This Equation presumes that there is no change in S_{conf} for temperatures lower than T_g^{12} . The value for the parameter A_e is a highly debated topic. This parameter represents the viscosity at infinite temperature (Toplis 1998) and is assumed to be constant for all silicate melts and thus independent of composition (Toplis et al. 1997; Giordano et al. 2008). In 1998, Toplis found $A_e = -2.6 \pm 1 \log_{10}$ Pa s. Russell et al. (2003) postulated this high temperature parameter to be $-3.2 \pm 0.66 \log_{10}$ Pa s for the Adam Gibbs theory. In a model from Giordano et al. (2008) the parameter is found to be $-4.55 \pm 0.21 \log_{10}$ Pa s as the optimal value. In more recent studies, Russell and Giordano (2017) set $A_e = -3.51 \pm 0.25 \log_{10}$ Pa s for their model and Robert et al. (2019) compared modelling with $A_e = -3.51 \log_{10}$ Pa s with a varying A_e . They conclude that a model with a variable A_e (-2.4 to $-4.0 \log_{10}$ Pa s) fits better to measured data. In this study, A_e is based on the Maxwell relation $\tau = \eta_0/G$ (with

τ —relaxation time, η_0 —time-independent Newtonian viscosity and G —elastic shear modulus) with $\tau_0 = 10^{-14}$ s (τ_0 is the vibration frequency at $T^{-1} = 0$) (Martinez and Angell 2001; Angell et al. 2003) and $G_\infty = 10 \pm 0.5$ GPa (G_∞ is the shear modulus at infinite frequency) (Dingwell and Webb 1989) and is calculated to be $-4.00 \log_{10}$ Pa s. This value lies in the range of the parameter discussed above. Parameters B_e and S_{conf} are fitted from the viscosity data using the calculated C_p^{conf} values after Giordano and Russell (2017) and the fixed A_e . Fitting the viscosity data to the Adam-Gibbs Equation allows the extrapolation of viscosity through temperature space from the low temperatures of the measurements to the high temperatures of geological processes.

A comparison of the fitted S_{conf} by Eq. 5 and the calculated S_{conf} after Russell and Giordano (2017) is seen in Fig. 10. The greatest deviations occur for PR-Leu and PR-CaO. However, all fitted values for S_{conf} (Eq. 5) are within the errors given by Russell and Giordano (2017). Hence, the correlation after Russell and Giordano (2017) works quite well for the studied melts. For further modelling processes, fitted S_{conf} after Eq. 5 are used.

The value for S_{conf} is lowest for the PR-0.7Fe composition ($17.26 \text{ J mol}^{-1} \text{ K}^{-1}$) and highest for PR-CaO ($35.98 \text{ J mol}^{-1} \text{ K}^{-1}$) as it is shown in Fig. 11 plotting S_{conf} vs γ .

The ratio B_e/S_{conf} is an indicator for the value of the changes of the average potential energy barrier to viscous flow (Richet 1984; Toplis 1998; Webb 2005) or the size of the smallest moving structural unit in the melt (Toplis 1998). This ratio is plotted against γ of the melts and shown in Fig. 12. It is highest for the PN compositions ($37.15 - 36.58 \times 10^3$ K), followed by PR-CaO (36.25×10^3 K), WPVe (35.86×10^3 K) and the PR series ($35.64 - 34.99 \times 10^3$ K) and the lowest B_e/S_{conf} ratio occurs for PR-Leu (34.52×10^3 K). This trend indicates that the size of the smallest structural unit in the melt decreases with decreasing polymerisation as the bridging oxygens are replaced by an increasing number of non-bridging oxygens.

Comparison with existing viscosity models

Several models exist for the prediction of the viscosity of silicate melts. Bottinga and Weill (1972) developed a model applying to many low viscosity extrusive anhydrous melts that was improved by Shaw (1972) to extend it to hydrous compositions. Giordano and Dingwell (2003) developed the first model considering the non-Arrhenian behaviour of silicate melts over a wide temperature range restricted to anhydrous melts. A model for anhydrous and hydrous silicate melts was given by Hui and Zhang (2007) expanding the temperature range for modelled viscosities. A further model was developed by Giordano et al. (2008) that encompasses most compositions of naturally occurring volcanic rocks and includes H_2O and F as volatile components. However, this

Fig. 10 Comparison of fitted S_{conf} using the Adam Gibbs model (Eq. 5) and the calculated ones after a correlation from Russel and Giordano (2017)

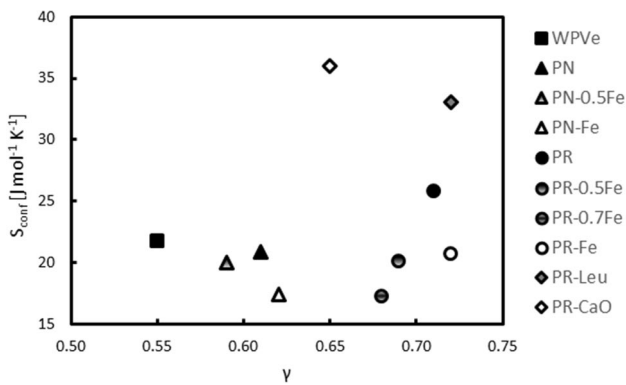
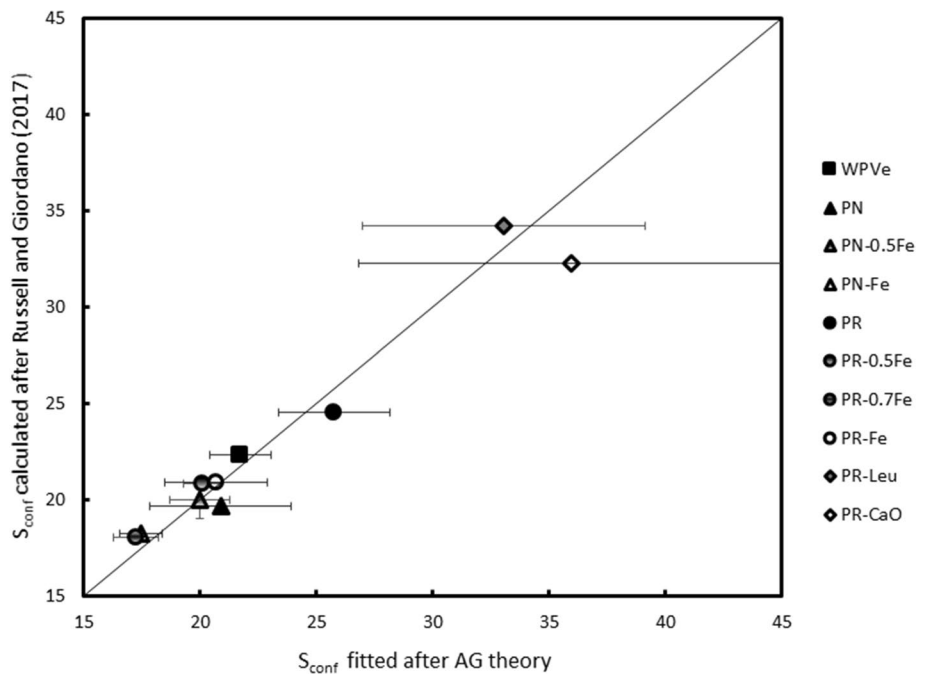


Fig. 11 S_{conf} fitted with Eq. 5 vs γ

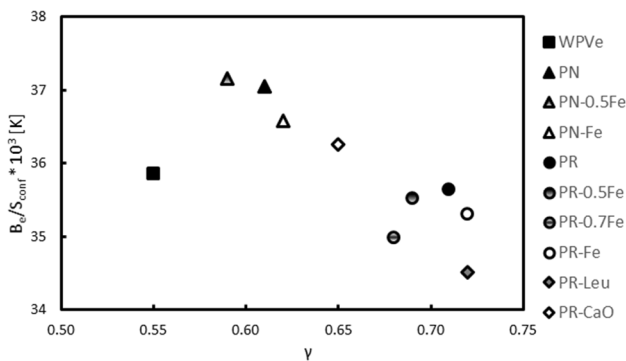


Fig. 12 $B_e/S_{conf} * 10^3$ vs γ

model does not differentiate between the iron species which affect the melt structure—and viscosity—in different ways. A model considering the iron speciation in common, iron-bearing melts was developed by Duan (2014) with a root-mean-square-error of 0.23 log units. Sehlke and Whittington (2016) developed a specific model for the anhydrous tholeiitic basalts taking into account the different iron species.

A comparison between measured and predicted viscosities in the range from $10^{8.3} \log_{10} \text{ Pa s}$ to $10^{13.5} \log_{10} \text{ Pa s}$, at temperatures from ~ 640 to ~ 840 °C, is done with the model from Hui and Zhang (2007) and shown in Fig. 13. This model underestimates the viscosities of the investigated melts with the highest iron content by approx. two and a half orders of magnitude (PR, PR-CaO, and PN and PR-Leu with FeO_{tot} of 9.46 wt%, 10.25 wt%, 7.28 wt% and 11.13 wt%, respectively, ordered with decreasing deviation). The lower the iron content the smaller the deviation. Whilst the viscosities of PN-0.5Fe and PR-0.5Fe are underestimated more than two orders in magnitude with decreasing deviations with increasing temperature, PR-0.7Fe is underestimated of approx. one order of magnitude at lower temperatures. When temperature rises the predicted viscosities for the PR-0.7Fe composition reach the measured viscosities. The predicted viscosity of the WPVe composition having the lowest iron content of all iron-bearing compositions (2.72 wt%) in this study is one $\log_{10} \text{ Pa s}$ lower than that measured at ~ 680 °C. At temperatures of ~ 720 °C and above, the measured viscosities of this melt are predicted quite well. The viscosities of the iron-free compositions PN-Fe and PR-Fe are within

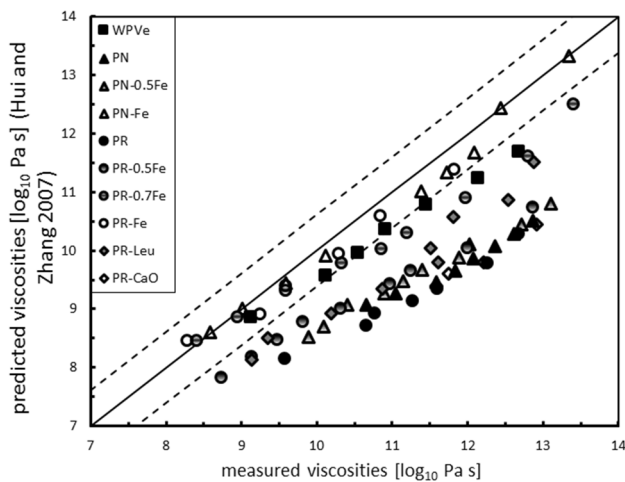


Fig. 13 Comparison of the measured viscosities in this study with those predicted by the model from Hui and Zhang (2007). Exact agreement is marked by the continuous line and upper and lower errors are marked by the dotted lines

the error of this model ($2\sigma = 0.61 \log_{10} \text{ Pa s}$) over the whole temperature range. This observation could be founded on the fact that the model from Hui and Zhang (2007) does not consider the iron speciation since it treats all iron as FeO. This is a very important criterion as ferrous and ferric iron have different effects on melt viscosity. Whereas ferrous iron is considered to act as a network modifier reducing the viscosity, ferric iron is assumed to behave like a network former and thus increases viscosity (i.e. Kress and Carmichael 1991; Wilke 2005; Knipping et al. 2015). Hence, the viscosity increasing influence of the ferric iron is completely disregarded by this model. Consequently, the higher the iron content of the studied melt (treated as FeO), the higher the total amount of ferric iron, the higher the network forming effect and the greater the underestimation of the prediction in viscosity as it is seen in Fig. 13. A second reason could be the dataset supporting this model includes a few phonolitic and tephritic compositions but no foiditic compositions.

The rheological data of this study are additionally compared with the model from Giordano et al. (2008) (subsequently denominated as GRD08) in Fig. 14. In the viscosity range from $10^{8.3}$ to $10^{13.3} \log \text{ Pa s}$, corresponding to temperatures of $\sim 680^\circ\text{C}$ to $\sim 840^\circ\text{C}$, the Fe-free melt compositions PN-Fe and PR-Fe and the WPVe melt composition ($\text{FeO}_{\text{tot}} < 3 \text{ wt}\%$) are predicted well by GRD08. The largest deviation is $0.32 \log \text{ Pa s}$, which is within its estimated error of 5%. In general, GRD08 underestimates the viscosities of most of the melts in this study, with the viscosity of the melt with the highest FeO_{tot} ($> 11 \text{ wt}\%$ for PR-Leu) underestimated by $\sim 1.25 \log_{10} \text{ Pa s}$. The viscosities for the PR-0.7Fe composition ($\text{FeO}_{\text{tot}} = 5.10 \text{ wt}\%$) are overestimated by up to one order in magnitude. In contrast, the viscosities for the

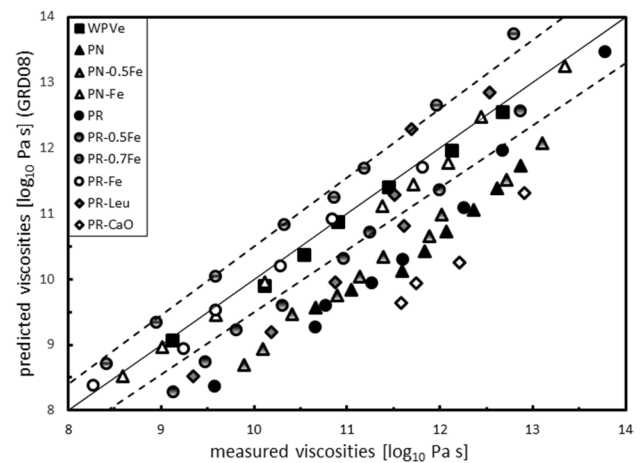


Fig. 14 Comparison of measured viscosities in this study with the predicted ones from Giordano et al. (2008). The continuous line represents exact agreement and dotted lines mark the upper and lower errors of the prediction given by GRD08

PN-0.5Fe composition with a similar FeO_{tot} content (5.82 wt%) are strongly underestimated by this model with deviations of $\sim 1.20 \log_{10} \text{ Pa s}$. The predicted viscosities of all other melt compositions are strongly underestimated. In particular, the prediction of viscosities of PR-CaO ($\text{FeO}_{\text{tot}} > 10 \text{ wt}\%$) is nearly 2 orders of magnitude lower than the measured ones. It is notable that the deviations of the predicted from the measured viscosities get smaller with decreasing iron content. One explanation could be that the GRD08 model does not take into account the iron speciation. The GRD08 model lists all iron as FeO_{tot} assuming the same $\text{Fe}^{2+}/\text{Fe}^{3+}$ ratio for all silicate melts, probably resulting in the underestimation of the viscosity of melts with more Fe^{3+} than that assumed in the general range of melt compositions used for fitting the model parameters. The model underestimates the viscosity of PR-0.5 Fe with $\text{Fe}^{2+}/\text{Fe}_{\text{tot}}$ of 0.36 but overestimates the viscosity of PR-0.7Fe with nearly the same $\text{Fe}^{2+}/\text{Fe}_{\text{tot}}$ of 0.37. So it can not be simply the $\text{Fe}^{2+}/\text{Fe}^{3+}$ ratio which results in an underestimation of the measured viscosities. A further possibility for the misfits of the GRD08 model could be that it is not calibrated for phonolitic or foiditic compositions investigated in this study.

Figure 15 shows a third comparison of the viscosities of the studied melt compositions with the model from Duan (2014) in the viscosity range from 10^9 Pa s to 10^{14} Pa s . The viscosity of most of the investigated melts (PR-Leu, PN-Fe, PR-0.7Fe, PR-0.5Fe and PR-Fe) are overestimated by this model up to $1.61 \log_{10} \text{ Pa s}$ for PR-Leu at $\sim 660^\circ\text{C}$. The viscosity of the WPVe composition is overestimated more than one order of magnitude at 680°C by this model. This overestimation decreases with increasing temperature to $0.23 \log_{10} \text{ Pa s}$ at 820°C . The predicted viscosities of the PR composition are overestimated with deviations of 0.63

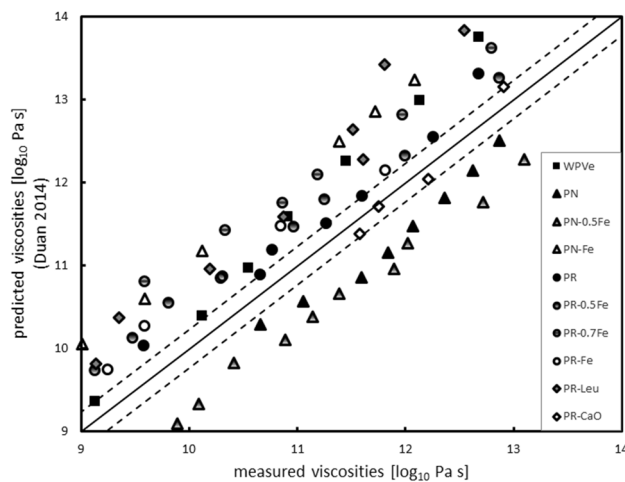


Fig. 15 Comparison of measured viscosities with predicted viscosities from the model from Duan (2014). The continuous line marks exact agreement and dotted lines mark the upper and lower error of the viscosity prediction

\log_{10} Pa s at 670 °C and $0.23 \log_{10}$ Pa s at 740 °C. The viscosity of the PR-CaO melt is quite well predicted within the given error of $0.23 \log_{10}$ Pa s. The viscosity of the PN and PN-0.5Fe compositions are underestimated over the whole viscosity range up to $0.73 \log_{10}$ Pa s and nearly one order in magnitude, respectively. The viscosity of the iron-rich and foiditic composition of the PR-CaO melt is the best prediction in this comparison although foiditic melt compositions are not included in the database for the model from Duan. Within the PN series it is seen that the predictions get worse with decreasing iron content. It is the same for PR, PR-0.5Fe and PR-0.7Fe. The model calibration is based on compositions showing a decreased iron content with increasing SiO₂ content not including all of the iron-silica-range of the melts in this study. Additionally, the model should not be used for iron-free compositions (Duan 2014). This point could be an explanation for the predicted viscosities within the PN series and PR, PR-0.5Fe and PR-0.7Fe getting worse with decreasing iron content but unchanged silica content.

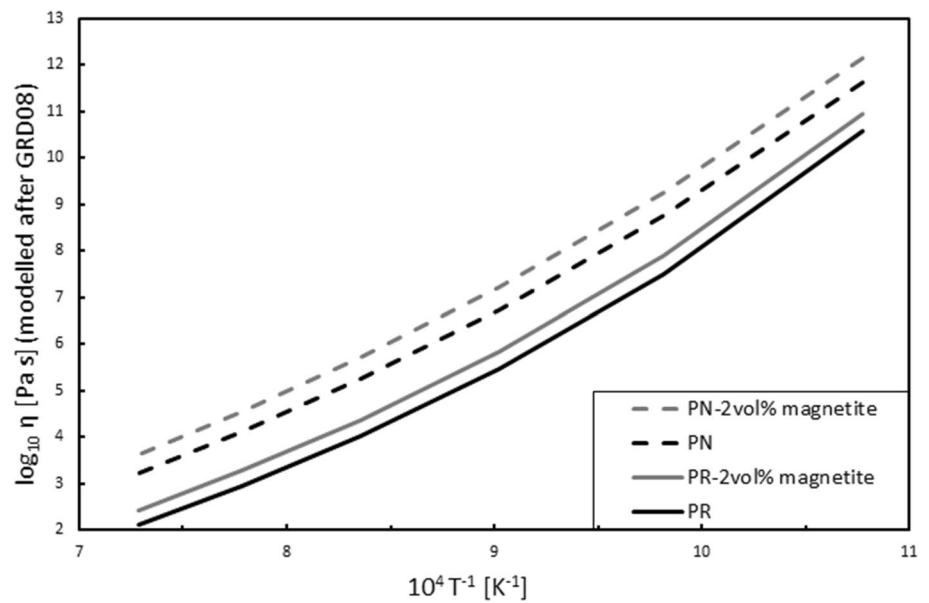
Commonly, higher viscosities than expected would occur in melts which contain crystals. X-ray diffraction of these glasses together with measurements of viscosity at alternating high and low temperature show that the melts are crystal-free. However, the Raman spectra after measurements show an increase in the nanolite content and a reduced “hump” typical for glass indicating a growth of nanolites (Fig. 4). Supposing a crystallisation of 2 vol% nano-magnetites, modelling the relative viscosity after Klein et al. (2018) considering the degree of crystallinity and the shape of crystals shows a viscosity increase of $0.03 \log_{10}$ Pa s. This influence is negligible since this change in viscosity is within the error of measurements. Nonetheless, the residual

liquid melt changes its composition during crystallisation and consequently its structure and rheological behaviour. The viscosity of the PN and PR composition in comparison with those after crystallisation of 2 vol% magnetite (PN-2 vol% magnetite and PR-2 vol% magnetite, respectively) is modelled using the GRD08 model. Due to the increased content of the network forming SiO₂, the depletion of Fe₃O₄ in the PN and PR melt increases the viscosity of the pure liquid melt by approx. $0.5 \log_{10}$ Pa s and nearly $0.4 \log_{10}$ Pa s, respectively, as demonstrated in Fig. 16. Consequently, the measured viscosities of the PN and PR melt differ from the actual viscosities since amounts of 1 to 2 vol% nano-magnetite are present in the melt. The viscosity increase due to crystallisation reduces the discrepancies between measured and predicted viscosities by the models of PN and PR melt. However, the viscosities are still underestimated by the model from Hui and Zhang (2007) and the GRD08 model. The predicted viscosity of the pure liquid PN composition after Duan (2014) converges to the predicted one whereas the predicted viscosity of the pure liquid PR compositions departs significantly from the predicted one. Furthermore, the modelled decrease in viscosity of the liquid PN melt of approx. $0.5 \log_{10}$ Pa s due to crystallisation of nanolites reduces the differences between the presented data and that of Campagnola et al. (2016).

Geology of the PN and PR eruptions

As mentioned above, the melt viscosity of the PR melt is lower than that of the PN melt (Fig. 5). Both melts have higher viscosities than expected based simply on the SiO₂ and K₂O contents (Fig. 2). The present data illustrate that the assimilation of the carbonate wall rock leads to a decrease in viscosity of the PR melt since the viscosities of PR-CaO are higher than those of the PR whole rock composition. This is not considering the effect of CO₂—that additionally enters the melt—on the melt viscosity during carbonate wall rock assimilation. Furthermore, the crystallisation of 4 mol % leucite from the PR whole rock composition leads to a decrease in viscosity of the residual melt PR-Leu. Depending on the crystal content, their shape, the connectivity between crystals in the melt, the resultant viscosity of a mixture of melt and crystals is higher than that of a crystal-free liquid and thus affecting the eruptive style (i.e. Stevenson et al. 1996; Caricchi et al. 2007; Vona et al. 2011). Caricchi et al. (2007) investigated the rheology of crystal-bearing magmas with a crystal fraction up to 80 wt%. Vona et al. (2011) studied the rheology of basaltic magmas with a crystal fraction up to approx. 30 vol%. Both studies present a model for calculating the apparent viscosity as a function of the applied shear rate. Following Kolzenburg et al. (2018), geological relevant shear rates range from approx. 70 s^{-1} to 10^{-9} s^{-1} .

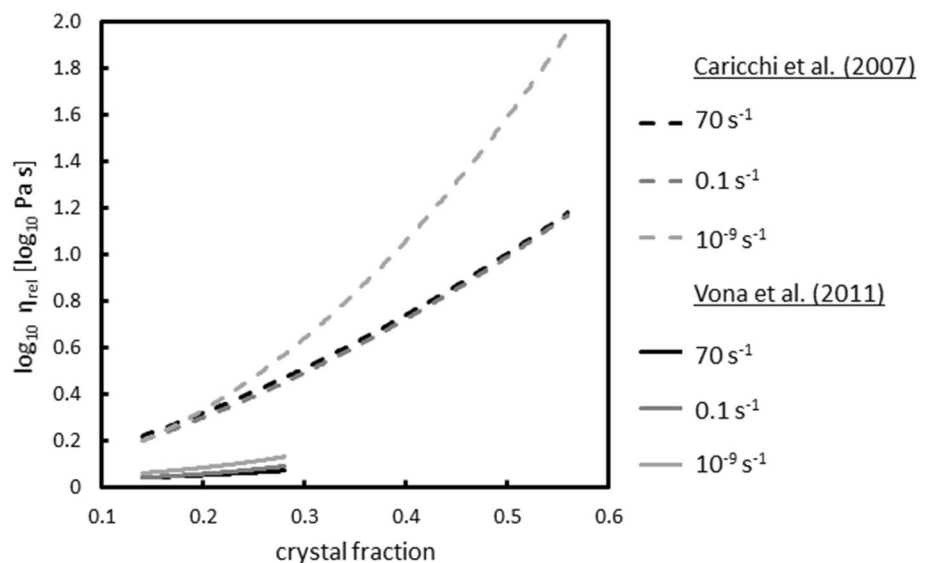
Fig. 16 Modelled liquid viscosities of the PN and PR composition and the PN and PR composition after the removal of 2 vol% magnetite after GRD08



Calculations of the relative viscosities depending on shear rate after Caricchi et al. (2007) and Vona et al. (2011) are presented in Fig. 17 with shear rates of 70 s^{-1} , 0.1 s^{-1} and 10^{-9} s^{-1} as a function of different leucite contents. 4 mol % leucite from the whole rock composition of PR correspond to ~14 vol% crystals in the melt. The volume of the melt was estimated after Lange and Carmichael (1987). As shown in Fig. 17, depending on the applied shear rate, the viscosity of the crystal bearing melt increases by 0.04 to 0.06 \log_{10} Pa s after Vona et al. (2011), which is negligible since it is within the error of the measurements but increases up to 0.22 \log_{10} Pa s after Caricchi et al. (2007). Freda et al. (2011) found some pyroclastic units from the PR event to be highly porphyric with leucite phenocrysts up to 40–60 vol%.

Therefore, the relative viscosity of two further leucite fractions are calculated for an approximation of the changes in viscosities: one with 28 vol% and another one with 56 vol% leucite crystals. The calculation after Vona et al. (2011) for a leucite fraction of 0.28 increases the viscosity by 0.13 \log_{10} Pa s in comparison to the model from Caricchi et al. (2007) that results in an increase of nearly 0.60 \log_{10} Pa s. Both models demonstrate higher relative viscosities with decreasing shear rates but show significant differences in predicting the relative viscosity with respect to each other. A leucite content of 56 vol% in the melt leads to a significant increase in viscosity up to nearly two orders in magnitude at a shear rate of 10^{-9} s^{-1} . However, these models do not consider the effect of magma evolution during crystallisation resulting in

Fig. 17 Relative viscosity η_{rel} vs leucite fraction. Two leucite fractions (0.14 and 0.28) are calculated after Caricchi et al. (2007) and Vona et al. (2011) and a third leucite fraction of 0.56 is calculated after Caricchi et al. (2007). Relative viscosities are calculated with three different shear rates (70 s^{-1} , 0.1 s^{-1} and 10^{-9} s^{-1}) relevant for volcanic implications



a depletion of K_2O – Al_2O_3 – SiO_2 from the melt composition. As shown in Fig. 5, the viscosity of the residual melt PR–Leu after 4 mol % leucite crystallisation decreases by nearly one order in magnitude. Assuming this behaviour continues during progressive crystallisation, the residual melt would become less viscous and the relative viscosity would not be as high as predicted by the models from Caricchi et al. (2007) and Vona et al. (2011).

Freda et al. (2011) discussed the PR event by plotting DRE vs. SiO_2 (Fig. 1) and observed that this low silica melt plots outside the cloud of data for large eruptions as a function of SiO_2 content. However, as shown in Fig. 18 this comparison is between Na_2O – K_2O -rich and CaO – MgO – FeO -rich melts.

As illustrated by the study of Webb et al. (2007), the viscosity of CaO – Al_2O_3 – SiO_2 melts is four orders of magnitude greater than that of Na_2O – Al_2O_3 – SiO_2 melts at 800 °C for $\gamma > 0.5$, with this difference decreasing with increasing temperature. Hess et al. (1995, 1996) also illustrate that the addition of 5 mol % CaO to a haplo-granitic composition melt results in a viscosity an order of magnitude higher than the composition with 5 mol % added Na_2O . Increasing these additions to 10 mol % produces a 2 order of magnitude difference between the Na_2O and CaO enriched melt viscosities. In contrast, the plot shown in Fig. 1 assumes the viscosities of the alkaline-earth rich PN and PR melts are similar to the low viscosity alkali-rich melts of the other eruptions in the graph. Figure 19 plots $(CaO + MgO)/(Na_2O + K_2O)$ vs SiO_2 content of several large-volume eruptions (see also Fig. 1). The PR composition appears to be an exception in this graph since it is the only melt with an alkaline-earth/alkaline ratio higher than 1. However, it follows an obvious trend of a decreasing $(CaO + MgO)/(Na_2O + K_2O)$ value with increasing SiO_2 content for all these events. Assuming

that this correlation is valid for more complex compositions, it illustrates that the viscosities of PR and PN compositions are higher than expected since their enrichment in alkaline earth is conventionally not considered in discussions of the viscosities of these melts. Thus, only regarding the SiO_2 content of a melt is insufficient for an estimation of its viscosity and rheological behaviour.

Trolese et al. (2017) investigated the emplacement temperatures of magmatic ignimbrites of the CAVD including the PN and PR eruptions. They found the emplacement temperature to be between 600 °C or 630 °C and 710 °C for PN and PR, respectively, and suggest that process of magma fragmentation begins at temperatures approx. 100 °C higher than the emplacement one. Takeuchi (2011) estimated pre-erupted temperatures for the other eruptions in Table 5 and Figs. 18, 20. With the presumption that melt fragmentation is a syn-eruptive process the eruptive temperatures for all compared melts range between 700 and 1070 °C. In this temperature range the viscosity curves of the PR and PN compositions cross the viscosity curves of the other Na_2O – Al_2O_3 – SiO_2 melts (Fig. 20) due to their different fragilities of ~31 and 24–28, respectively.

In January 2002, foiditic lava was ejected by the Mt. Nyiragongo (Santo et al. 2002; Giordano et al. 2007). The lava near the top of the volcano was highly fluid and moved quickly forward whereas the lava at the bottom of Mt. Nyiragongo was more viscous moving with less speed. Giordano et al. (2007) measured the dry liquid viscosity of remelted lava from this eruption to be approx. two \log_{10} Pa s lower than that from the foiditic synthetic glasses from this study. They conclude different eruptive temperatures at the different locations: the lava escaped in higher altitudes erupted at higher temperatures than the lava at the base of the volcano resulting in a lower viscous flow near

Fig. 18 Net diagram for the investigated PR, PN and WPVe compositions and other large-volume eruptions worldwide. Compositions are in mol % ranging from 0 mol % up to 15 mol % at the outermost line. The compositions analysed in this study are rich in potassium and the PR and PN compositions have much higher contents in FeO_{tot} , MgO and especially CaO in comparison with the other melts. The Laacher See composition is enriched in Na_2O . For detailed information of the compositions see Table 1 (for PR, PN and WPVe) or Takeuchi (2011) and references therein (for the other eruptions)

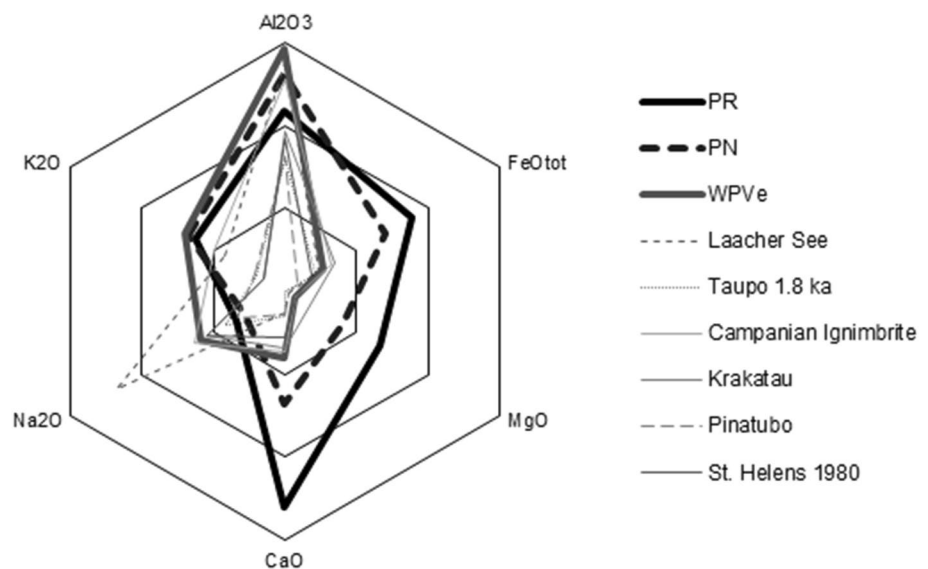


Fig. 19 Comparison of high-volume eruptions in the plot (CaO + MgO)/(Na₂O + K₂O) vs SiO₂

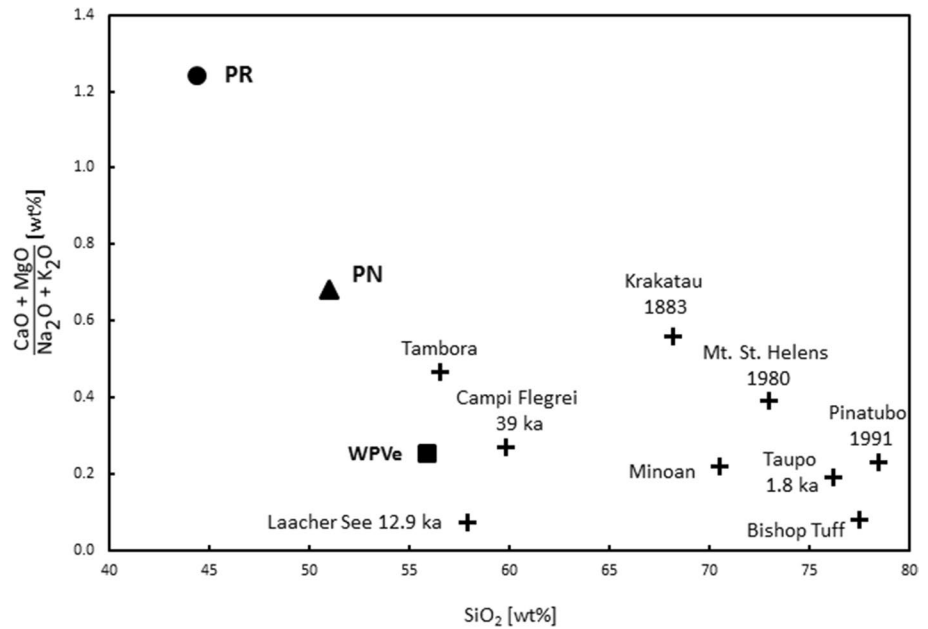


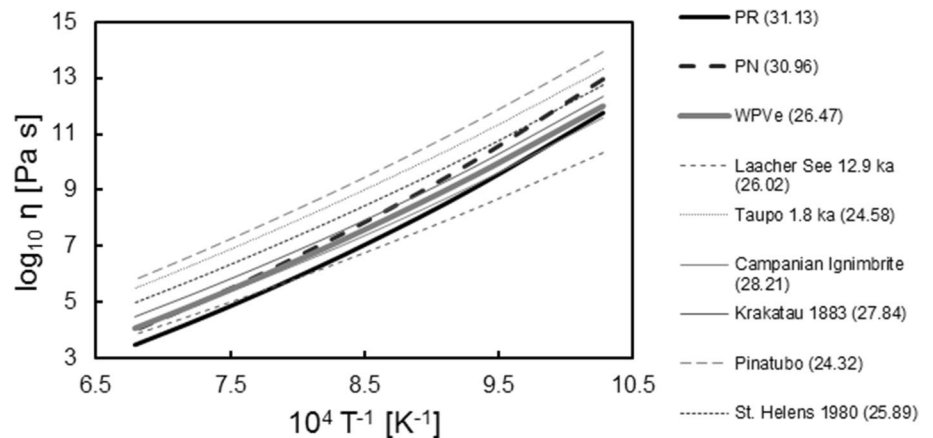
Table 5 Chemical classification and fragilities from large-volume eruptions from all over the world

Explosive event	Composition	References	Fragility
PR	Foidite	Freda et al. (2011)	31.13 ^a
PN	Tephri-phonolite	Campagnola et al. (2016)	30.96 ^a
WPVe	Phonolite	Balcone-Boissard et al. (2011) Iacono-Marziano et al. (2007a, b)	26.47 ^a
Laacher See	Phonolite	Harms and Schmincke (1999)	26.02 ^b
Taupo 1.8 ka	Rhyolitic	Dunbar et al. (1989)	24.58 ^b
Campanian Ignimbrite	Trachytic	Marianelli et al. (2006)	28.21 ^b
Krakatau	Mainly rhyodacitic	Mandeville et al. (1996)	27.84 ^b
Pinatubo 1991	Dacitic	Westrich and Gerlach (1992)	24.32 ^b
Usu 1663	Rhyolitic	Tomiya et al. (2010)	25.31 ^b
Aniakchak 3430 BP	Andesitic	Larsen (2006)	34.95 ^b
St. Helens 1980	Rhyolitic	Takeuchi (2011)	25.89 ^b

^aFragility calculated after Eq. 4

^bFragility calculated after GRD08 (Giordano et al. 2008)

Fig. 20 Viscosities of the PR, PN and WPVe compositions investigated in this study with measured and extrapolated viscosities using Eq. 5 and further large-volume eruptions worldwide. Compositions for these events are taken from Takeuchi and references therein (2011), viscosities are calculated with the GRD08 model. Fragilities are written in parentheses



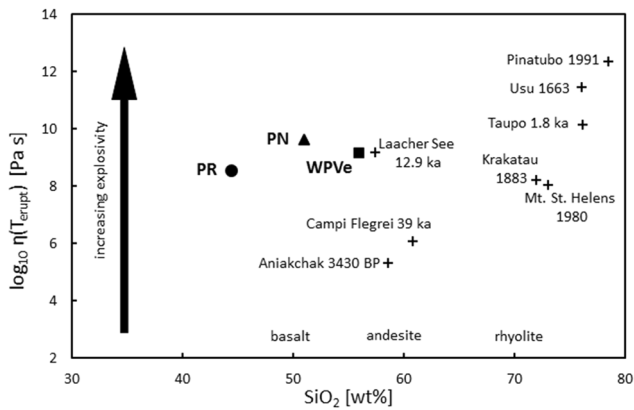


Fig. 21 Viscosity at eruptive temperature as a function of SiO₂ content for some large-volume eruptions showing that the eruptive viscosities for PR, PN and WPVe are in the middle of all these explosive events

the volcanic top. The eruptive temperatures for the Mt. Nyiragongo event are much higher than those for the PR event what results in higher eruptive viscosity for PR.

Consequently, as an approximation of the rheology of an erupting magma controls the explosivity of an eruptive event, the viscosity at the eruptive temperature ($\eta(T_{\text{erupt}})$) should be regarded rather than the SiO₂ content only. In Fig. 21, the viscosity at the temperature at eruption is plotted vs the silica content for some of the major explosive eruptions with a high DRE. The viscosities at eruptive temperature from the melts from literature are calculated with the GRD08 model ignoring any content of H₂O. The PR, PN and WPVe compositions measured in this study have eruptive viscosities of 8.58, 9.56 and 9.18 log₁₀ Pa s, respectively. It is seen that their eruptive viscosities are in the middle of all events in spite of their low SiO₂ content. The explosivity of an eruption increases with increasing eruptive viscosity. By means of this plot it can be estimated that at eruptive viscosities of 5–6 log₁₀ Pa s the eruptive style changes from effusive to explosive considering a dry and crystal- and bubble-free magma. The relationship between the DRE of all these explosive events and the eruptive temperature is shown in Fig. 22, indicating that these eruptions fall together in the same area in this figure and that the PR and PN events are also in the middle of all data points. Considering the melt viscosity at the eruption of an event, the PR and PN eruptions are not as unusual as they appear when plotted in the DRE vs SiO₂ diagram (Fig. 1).

However, natural magmas and lavas are a mixture of a liquid melt, solid particles and gas bubbles (Lev et al. 2019). This, together with the species of volatiles, strain and shear-rates generated by the geological setting of a volcano, results in a complex melt rheology (i.e. Dingwell et al. 1996; Giordano et al. 2008; Robert et al. 2013; Sehlke and Whittington 2016) not investigated in this study. Especially

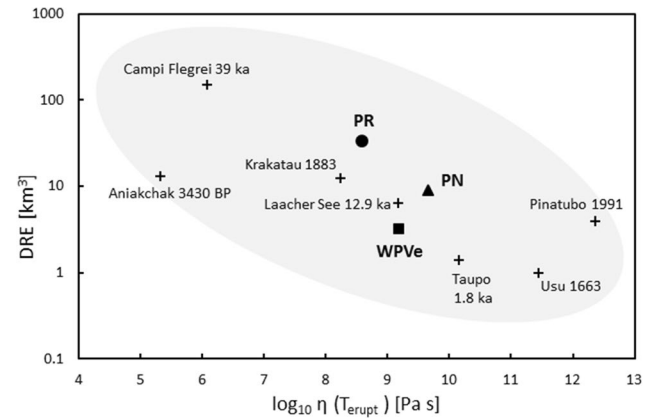


Fig. 22 DRE from explosive eruptions as a function of the viscosity at eruptive temperature. PR, PN and WPVe form a cloud with the other eruptions showing no anomalous position

for the geological conditions of the CAVD, the formation of a CO₂-rich fluid and an enrichment of the CaO component in the melt even in syn-eruptive processes are important features affecting the style of its eruptions.

Nevertheless, the plot in Fig. 19 constitutes a good first approximation of the explosivity of an eruption including the alkali-earth content as well as the SiO₂ content.

Conclusion

Considering the SiO₂ content only or together with the alkali content is a common way to estimate the viscosity of a melt. This study illustrates that this is not sufficient. The viscosities presented here are higher than expected using conventional approximations as these compositions are not only silica undersaturated and rich in K but also rich in alkaline earths. The knowledge of the rheological features of a melt and especially the viscosity is fundamental for understanding and evaluating the style in which a volcano erupts. Hence, it is proposed here to estimate the explosivity of an eruption not only based on the silica content of a melt but additionally on the ratio (CaO + MgO)/(Na₂O + K₂O).

Acknowledgments Open Access funding provided by Projekt DEAL.

Open Access This article is licensed under a Creative Commons Attribution 4.0 International License, which permits use, sharing, adaptation, distribution and reproduction in any medium or format, as long as you give appropriate credit to the original author(s) and the source, provide a link to the Creative Commons licence, and indicate if changes were made. The images or other third party material in this article are included in the article's Creative Commons licence, unless indicated otherwise in a credit line to the material. If material is not included in the article's Creative Commons licence and your intended use is not permitted by statutory regulation or exceeds the permitted use, you will

need to obtain permission directly from the copyright holder. To view a copy of this licence, visit <http://creativecommons.org/licenses/by/4.0/>.

References

- Adam G, Gibbs JH (1965) On the temperature dependence of cooperative relaxation properties in glass-forming liquids. *J Chem Phys* 43:139–146
- Anderson AT Jr, Newman S, Williams SN, Drits TH, Skirius C, Stolper E (1989) H₂O, CO₂, Cl and gas in Plinian and ash-flow Bishop rhyolite. *Geology* 17:221–225
- Angell CA, Yue Y, Wang L-M, Colpey JRD, Borick S, Mosa S (2003) Potential energy, relaxation, vibrational dynamics and boson peak, of hyperquenched glasses. *J Phys: Condensed Matter* 15:1051–1068
- Balcone-Boissard H, Boudon G, Villemant B (2011) Textural and geochemical constraints on eruptive style of the 79 AD eruption at Vesuvius. *Bull Volcanol* 73:279–294
- Blythe LS, Deegan FM, Freda C, Jolis EM, Masotta M, Misiti V, Taddeucci J, Troll VR (2015) CO₂ bubble generation and migration during magma-carbonate interaction. *Contrib Mineral Petrol* 169:42
- Boari E, Avanzinelli R, Melluso L, Giordano G, Mattei M, De Benedetti AA, Morra V, Conticelli S (2009) Isotope geochemistry (Sr-Nd-Pb) and petrogenesis of leucite-bearing volcanic rocks from “Colli Albani” volcano, Roman Magmatic Province, Central Italy: inferences on volcano evolution and magma genesis. *Bull Volcanol* 71:977–1005
- Bottinga Y, Weill DF (1972) The viscosity of magmatic silicate liquids: a model for calculation. *Am J Sci* 272:438–475
- Campagnola S, Vona A, Giordano G (2016) Crystallization kinetics and rheology of leucite-bearing tephriphonolite magmas from the Colli Albani volcano (Italy). *Chem Geol* 424:12–29
- Caricchi L, Burlini L, Ulmer P, Gerya T, Vassalli M, Papale P (2007) Non-Newtonian rheology of crystal-bearing magmas and implications for magma ascent dynamics. *Earth Planet Sci Lett* 264:402–419
- Chiarabba C, Amato A, Delaney PT (1997) Crustal structure, evolution, and volcanic unrest of the Alban Hills, Central Italy. *Bull Volcanol* 59:161–170
- Di Genova D, Sicola S, Romano C, Vona A, Fanara S, Spina L (2017) Effect of iron and naolites on Raman spectra of volcanic glasses: a reassessment of existing strategies to estimate the water content. *Chem Geol* 475:76–86
- Di Rocco T, Freda C, Gaeta M, Mollo S, Dallai L (2012) Magma chambers emplaced in carbonate substrate: petrogenesis of skarn and cumulate rocks and implications for CO₂ Degassing in Volcanic Areas. *J Petrology* 53:2307–2332
- Dingwell DB, Webb SL (1989) Structural Relaxation in Silicate Melts and Non-Newtonian Melt Rheology in Geological Processes. *Phys Chem Minerals* 16:508–516
- Dingwell DB, Knoche R, Webb SL (1992) The effect of B₂O₃ on the viscosity of haplogranitic liquids. *Am Mineral* 77:457–461
- Dingwell DB, Romano C, Hess K-U (1996) The effect of water on the viscosity of a haplogranitic melt under P-T-X conditions relevant to silicic volcanism. *Contrib Mineral Petrol* 124:19–28
- Duan X (2014) A model for calculating the viscosity of natural iron-bearing silicate melts over a wide range of temperatures, pressures, oxygen fugacities and compositions. *Am Mineral* 99:2378–2388
- Dunbar NW, Hervig RL, Kyle PR (1989) Determination of pre-eruptive H₂O, F and Cl contents of silicic magmas using melt inclusions: examples from Taupo volcanic center, New Zealand. *Bull Volcanol* 51:177–184
- Einstein A (1906) Eine neue Bestimmung der Moleküldimensionen. *Annals Phys* 19:289–306
- Falenty K, Webb SL (2010) Shear modulus, heat capacity, viscosity and structural relaxation time of Na₂O-Al₂O₃-SiO₂ and Na₂O-Fe₂O₃-Al₂O₃-SiO₂ melts. *Phys Chem Minerals* 37:613–634
- Freda C, Gaeta M, Misiti V, Mollo S, Dilfi D, Scarlato P (2008) Magma-carbonate interaction: an experimental study on ultrapotassic rocks from Alban Hills (Central Italy). *Lithos* 101:397–415
- Freda C, Gaeta M, Giaccio B, Marra F, Palladino DM, Scarlat P, Sottili G (2011) CO₂-driven large mafic explosive eruptions: the Pozzolane Rosse case study from the Colli Albani Volcanic District (Italy). *Bull Volcanol* 73:241–256
- Gaeta M, Freda C, Marra F, Arienzo I, Gozzi F, Jicha B, Di Rocco T (2016) Paleozoic metasomatism at the origin of Mediterranean ultrapotassic magmas: constraints from time-dependent geochemistry of Colli Albani volcanic products (Central Italy). *Lithos* 244:151–164
- Giordano D, Dingwell DB (2003) Non-Arrhenian multicomponent melt viscosity: a model. *Earth Planet Sci Lett* 208:337–349
- Giordano D, Russell JK (2017) The heat capacity of hydrous multicomponent natural melts and glasses. *Chem Geol* 461:96–103
- Giordano G, De Benedetti AA, Diana A, Diano G, Gaudio F, Marsasco F, Miceli M, Mollo S, Cas RAF, Funicello R (2006) The Colli Albani mafic caldera (Roma, Italy): stratigraphy, structure and petrology. *J Volcanol Geotherm Res* 155:49–80
- Giordano D, Polacci M, Longo A, Papale P, Dingwell DB, Boschi E, Kasereka M (2007) Thermo-rheological magma control on the impact of highly fluid lava flows at Mt. Nyiragongo. *Geophys Res Lett* 34:L06301
- Giordano D, Russell JK, Dingwell DB (2008) Viscosity of magmatic liquids: a model. *Earth Planet Sci Lett* 271:123–134
- Harms E, Schmincke H-U (1999) Volatile composition of the phonolitic Laacher See magma (12,900 yr BP): implications for syn-eruptive degassing of S, F, Cl and H₂O. *Contrib Mineral Petrol* 138:84–98
- Hess K-U, Dingwell DB, Webb SL (1995) The influence of excess alkalis on the viscosity of a haplogranitic melt. *Am Mineral* 80:297–304
- Hess K-U, Dingwell DB, Webb SL (1996) The influence of alkaline-earth oxides (BeO, MgO, CaO, SrO, BaO) on the viscosity of a haplogranitic melt: systematics of non-Arrhenian behaviour. *Eur J Mineral* 8:371–381
- Hui H, Zhang Y (2007) Toward a general viscosity equation for natural anhydrous and hydrous silicate melts. *Geochim Cosmochim Acta* 71:403–416
- Iacono Marziano G, Schmidt BC, Dolfi D (2007) Equilibrium and disequilibrium degassing of a phonolitic melt (Vesuvius AD 79 “white pumice”) simulated by decompression experiments. *J Volcanol Geotherm Res* 161:151–164
- Iacono-Marziano G, Gaillard F, Pichavant M (2007) Limestone assimilation and the origin of CO₂ emissions at the Alban Hills (Central Italy): constraints from experimental petrology. *J Volcanol Geotherm Res* 166:91–105
- Karner DB, Marra F, Renne PR (2001) The history of the Monte Sabatini and Alban Hills volcanoes: groundwork for assessing volcanic-tectonic hazards for Rome. *J Volcanol Geotherm Res* 107:185–219
- Klein J, Mueller SP, Helo C, Schweitzer S, Gurioli L, Castr JM (2018) An expanded model and application of the combined effect of crystal-size distribution and crystal shape on the relative viscosity of magmas. *J Volcanol Geotherm Res* 357:128–133
- Knipping JL, Behrens H, Wilke M, Göttlicher J, Stabile P (2015) Effect of oxygen fugacity on the coordination and oxidation state of iron in alkali bearing silicate melts. *Chem Geol* 411:143–154

- Kolzenburg S, Di Genova D, Giordano D, Hess KU, Dingwell DB (2018) The effect of oxygen fugacity on the theological evolution of crystallizing basaltic melts. *Earth Planet Sci Lett* 487:21–32
- Kress VC, Carmichael ISE (1991) The compressibility of silicate liquids containing Fe_2O_3 and the effect of composition, temperature, oxygen fugacity and pressure on their redox state. *Contrib Mineral Petrol* 108:82–92
- Lange RA, Carmichael ISE (1987) Densities of Na_2O - K_2O - CaO - MgO - FeO - Fe_2O_3 - Al_2O_3 - TiO_2 - SiO_2 liquids: new measurements and derived partial molar properties. *Geochim et Cosmochim Acta* 51:2931–2946
- Larsen JF (2006) Rhyodacite magma storage cobdittins prior to the 3430 yBP caldera-forming eruption of Aniakchak volcano, Alaska. *Contrib Mineral Petrol* 152:523–540
- Lev E, Rumpf E, Dieterich H (2019) Analog experiments of lava flow emplacement. *Ann Geophys* 62:2
- Maier CG, Kelley KK (1932) An equation for the representation of high-temperature heat content data. *J Am Chem Soc* 54:3243–3246
- Mandeville CW, Carey S, Sigurdsson H (1996) Magma mixing, fractional crystallization and volatile degassing during the 1883 eruption of Krakatau volcano, Indonesia. *J Volcanol Geotherm Res* 74:243–274
- Marianelli P, Sbrana A, Proto M (2006) Magma chamber of the Campi Flegrei supervolcano at the time of eruption of the Campanian Ignimbrite. *Geol Soc Am* 34:937–940
- Marra F, Karner DB, Freda C, Gaeta M, Renne P (2009) Large mafic eruptions on Alban Hills Volcanic District (Central Italy): chronostratigraphy, petrography and eruptive behaviour. *J Volcanol Geotherm Res* 179:217–232
- Marsh BD (1981) On the crystallinity, probably occurrence, and rheology of lava and magma. *Contrib Mineral Petrol* 78:85–98
- Martinez L-M, Angell CA (2001) A thermodynamic connection to the fragility of glass-forming liquids. *Nature* 410:663–667
- Peccerillo A (2005) Plio-quaternary volcanism in Italy petrology, geochemistry, geodynamics. Springer, Berlin Heidelberg, p 365
- Pocklington HC (1940) Rough measurement of high viscosities. *Proc Cambridge Phil Soc* 36:507–508
- Richet P (1984) Viscosity and configurational entropy of silicate melts. *Geochim Cosmochim Acta* 48:471–483
- Richet P (1987) Heat capacity of silicate glasses. *Chem Geol* 62:111–124
- Robert G, Whittington AG, Stechern A, Behrens H (2013) The effect of water on the viscosity of synthetic calc-alkaline basaltic andesite. *Chem Geol* 346:135–148
- Robert G, Smith RA, Whittington AG (2019) Viscosity of melts in the NaAlSiO_4 - SiO_2 system: configurational entropy modelling. *J Non-Cryst Solids* 524:119635
- Robie RA, Hemingway BS, Fischer JR (1978) Thermodynamic properties of minerals and related substances at 29815 K and 1 bar (10^5 Pa) pressure and at higher temperatures. *US Geol Surv Bull* 1452:428–446
- Roscoe R (1952) The viscosity of suspensions of rigid spheres. *Br J Appl Phys* 3:267–269
- Russel JK, Giordano D (2017) Modelling configurational entropy of silicate melts. *Chem Geol* 461:140–151
- Russel JK, Giordano D, Dingwell DB (2003) High-temperature limits on viscosity of non-Arrhenian silicate melts. *Am Mineral* 88:1390–1394
- Santo AP, Capaccioni B, Tedesco D, Vaselli O (2002) Petrographic and geochemical features of the 2002 Nyiragongo lava flows. *Acta Vulcanol* 14:63–66
- Schuessler JA, Botcharnikov RE, Behrens H, Misiti V, Freda C (2008) Oxidation state of iron in hydrous phono-tephritic melts. *Am Mineral* 93:1493–1504
- Sehlke A, Whittington AG (2016) The viscosity of planetary tholeiitic melts: a configurational entropy model. *Geochim Cosmochim Acta* 191:277–299
- Shand SJ (1927) *The eruptive rocks*. Wiley, New York NY
- Shaw HR (1972) Viscosities of magmatic silicate liquids, an empirical method of prediction. *Am J Sci* 272:870–893
- Stevenson RJ, Dingwell DB, Webb SL, Sharp TG (1996) Viscosity of microlite-bearing rhyolitic obsidians: an experimental study. *Bull Volcanol* 58:298–309
- Takeuchi S (2011) Preeruptive magma viscosity: an important measure of magma eruptibility. *J Geophys Res* 116:B10201
- Tobolsky AV, Taylor RB (1963) Viscoelastic properties of a simple organic glass. *J Phys Chem* 67:2439–2442
- Tomiya A, Takahashi E, Furukawa N, Suzuki T (2010) Depth and evolution of a silicic magma chamber: melting experiments on a low-K Rhyolite from Usu Volcano, Japan. *J Petrol* 51:1333–1354
- Toplis MJ (1998) Energy barriers to viscous flow and the prediction of the glass transition temperatures of molten silicates. *Am Mineral* 83:480–490
- Toplis MJ, Dingwell DB, Hess K-U, Lenci T (1997) Viscosity, fragility and configurational entropy of melts along the join SiO_2 - NaAlSiO_4 . *Am Mineral* 82:979–990
- Trolese M, Giordano G, Cifelli F, Winkler A, Mattei M (2017) Forced transport of thermal energy in magmatic and phreatomagmatic large volume ignimbrites: paleomagnetic evidence from the Colli Albani volcano, Italy. *Earth Planet Sci Lett* 478:179–191
- Vona A, Romano C, Dingwell DB, Giordano D (2011) The rheology of crystal-bearing basaltic magmas from Stromboli and Etna. *Geochim Cosmochim Acta* 75:3214–3236
- Webb SL (2005) Structure and rheology of iron-bearing Na_2O - Al_2O_3 - SiO_2 melts. *Eur J Mineral* 17:223–232
- Webb SL (2008) Configurational heat capacity of Na_2O - CaO - Al_2O_3 - SiO_2 melts. *Chem Geol* 256:92–101
- Webb SL (2011) Configurational heat capacity and viscosity of (Mg, Ca, Sr, Ba)- Al_2O_3 - SiO_2 melts. *Eur J Mineral* 23:487–497
- Webb SL (2014) Rheology and the Fe^{3+} -chlorine reaction in basaltic melts. *Chem Geol* 366:24–31
- Webb SL, Müller E, Büttner H (2004) Anomalous rheology of peraluminous melts. *Am Mineral* 89:812–818
- Webb SL, Banaszak M, Köhler U, Rausch S, Raschke G (2007) The viscosity of Na_2O - CaO - Al_2O_3 - SiO_2 melts. *Eur J Mineral* 19:681–692
- Westrich HR, Gerlach TM (1992) Magmatic gas source for the stratospheric SO_2 cloud from the June 15, eruption of Mount Pinatubo. *Geology* 20:867–870
- Whittington A, Richet P, Holtz F (2000) Water and viscosity of depolymerized aluminosilicate melts. *Geochim Cosmochim Acta* 64:3725–3736
- Wilke M (2005) Fe in magma—an overview. *Ann Geophys* 48:609–617
- Wilson AD (1960) The Micro-determination of Ferrous Iron in Silicate Minerals by a Volumetric and a Colorimetric Method. *Analyst* 85:823–827

Publisher's Note Springer Nature remains neutral with regard to jurisdictional claims in published maps and institutional affiliations.